Identification of blowing snow particles in images from a multi-angle snowflake camera

The Cryosphere #tc-2018-248

M. Schaer, C. Praz and A. Berne

November 21, 2019

Responses to reviewers (2)

We thank the reviewers for their constructive comments which helped improve the second revised version of the manuscript. In the present document, we provide our responses to the comments of the two reviewers. The comments of the reviewers are reported in *italic*, our responses in normal font and the corresponding modifications in the manuscript in blue. Page and line numbers referred to in our responses correspond to the version with changes highlighted.

Reviewer 1

General comments

1. *I have read the new version of the manuscript and the answers of the authors to the first round of review. The authors addressed well the main points raised in the first round of review and this improved the quality of the paper. In particular, I enjoyed reading the extended section presenting results that illustrates well the potential of the method developed by the authors. Therefore, I recommend this paper to be accepted for publication in TC. I made below a few comments that the authors should consider prior to publication.*

   We thank Reviewer 1 for this positive evaluation.

Technical comments

1. *P4 L 2: SPC are carrying out measurements at frequency higher than 1 HZ. Nishimura et al. (2014) used the high-frequency sampling ability of the SPC to determine the speed of particles during blowing snow events. I recommend the authors to add here something on the high-frequency sampling ability of the SPC.*

   We have modified the text as follows:
   ...particle mass flux usually at a 1-s resolution (but raw data are measured at up to 150 kHz,

Nishimura et al., 2014).

2. *P7 L 3-7: The characteristics of the MASC has already been described in Section 2.1 and this paragraph could be shortened.*

   We have shortened the text as follows:
   The MASC instrument and the collected images are described in Section 2.1.

3. *P 7 L 27: replace "ground surface" by "snow surface".*

   Done.

4. *P 13 Fig. 7: The graphs are very hard to read. Indeed, it is hard to identify the False positive and False negative due to their restricted numbers. For some of the plots, the GMM contours are also hardly visible. It would be very good the authors could make this figure easier to read prior to publication.*

   We have modified Fig.7 to improve its readability. It remains a figure with a lot of information...

5. *P 18 L1: The occurrence of blowing snow in alpine terrain presents a strong variability due to the influence of the topography on the atmospheric flow. Results would be certainly different if the MASC had been placing on one of the crests surrounding the Weissflujoch.*

   We agree with the Reviewer that we expect more blowing snow near the crests in an alpine terrain. Our point here is however to highlight the fact that even within a structure designed to minimize wind effects on solid precipitation (the DFIR), we still see blowing snow occurrence in the MASC data.

6. *P 19 Fig 12: Were these images obtained after application of the median filter? The 3 aligned white dots on the left images suggested that it is not the case. If possible, I recommend the authors to show the filtered images here.*

   We have modified the figure to display the binary images obtained after filtering.

7. *P 23, L14: Missing "," between "GMM" and "too coarse".*

   Added.

Reviewer 2

We thank very much Reviewer 2 for their in-depth and detailed evaluation of our manuscript, which helped us clarify important aspects.

General comments

1. *Primarily, it is as of yet unclear to me whether or not this Gaussian mixture method is necessary or beneficial for categorizing images. Figs 6 and 7, and to some point Figure 14 seem to suggest that the dominate separating factor for the two end-states is the image frequency. Though there is a low finite upper limit on this frequency, this is a loose proxy for snow particle flux in much the same way as a particle counter gives you an index of how many times a sensor is triggered. Physically, it makes sense for the snow flux to differentiate these two regimes as the settling velocity of falling particles is much lower than potential transport speeds, and the potential rates of snow transport by the two methods are quite different. That being said, it would benefit the manuscript greatly if the authors could show that all the technical machinery of the Gaussian mixture model and the addition of the other image analysis metrics (Distance Transform, Squared fractal index, Dmax) are indeed necessary to have accuracy at this order of magnitude and that they are not superfluous technical additions. Other advantages that I may have overlooked would also benefit from being highlighted more.*

   This is an important point, and we thanks the reviewer for raising it so we can better explain and clarify our approach. As illustrated by the S values in Table 2 and the distributions in Fig. 6, 7 and 14, the image frequency is the most informative feature to distinguish blowing snow and precipitation images. But it must be noted that these values and figures correspond to the training set, composed of selected images of pure blowing snow and pure precipitation. For these "pure" cases, the image frequency would be enough to separate the two types. But when considering all types of images, including pure blowing snow and pure precipitation but also mixture of the two, then the other features contribute to the classification. This is implicitly visible in Fig. 12: the time interval between the top left image (mixed towards blowing snow) and the top right one (pure blowing snow) is about 4 s, 3 s between the top right and the bottom left (pure precipitation), and less than 1 sec between the bottom left and bottom right (mixed towards precipitation). The image frequency is hence similar and even larger for the transition between pure precip and mixed precip. So the difference in the outcome is explained by the other features used for the classification, illustrating their importance for the mixed cases in particular.
   We have added the following text in the comment of Fig. 12:
   (and hence the contribution of the features other than image frequency).

2. *I think it would be illuminating for a broader audience and enhance the transparency of the manuscript if it was clearly acknowledged that the normalized angle does not actually give any indication of what proportion of a given image is blowing snow versus precipitation, but actually only indicates what the probability is that an image is one of the two end states according to their training data. As the methods are currently described, this is my understanding of the Gaussian mixture model output. If this is inaccurate, it would also be of benefit to rectify future misunderstandings with further clarification. Furthermore, for technical the paper is,*

the validation appears to be largely qualitative, with a tendency towards arguing "typically there is more blowing snow here than there.."

The Reviewer is right in that the normalized angle corresponds to a probability that a given mixed image is closer to pure blowing snow (normalized angle close to 1) or pure precipitation (normalized angle close to 0).
We have added the following text in the description of the normalized angle after Eq.7:
of the considered image (and not the respective proportions within this image)

Concerning validation and its qualitative nature, the Reviewer may be confused between the quantitative validation of the fitted GMM performed using the training set (end of Section 4.2, Fig.8) and the application of the proposed method to the entire data sets from the Alps and from Antarctica (Section 5), the evaluation of which is qualitative by essence as we do not have reference data. For the specific aspect of the quantitative evaluation of the mixing index (related to the normalized angle), we similarly do not have reference data to compare to... But it is important to remember that the normalized angle is based on a distance to the cluster centroids, so it is not completely arbitrary.

Specific comments

1. *P2L4-10: This drifting versus blowing snow designation is unnecessary, and the authors are inconsistent in the use of it. The more technical modes of creep, saltation, and suspensions would be more appropriate differentiations.*

   We have modified this paragraph into:
   Ice particles moving at the snow surface belong to one of the three main types of associated motion: creep, saltatation and suspension (e.g. Kind, 1990). Given the fact that the observations used in the present study were collected about 3 m above the ground (or snow surface) level, the term "blowing snow" hereinafter refers to wind-suspended ice particles.

2. *P2L18-20: Please refrain from saying obviously as it undervalues the work.*

   We changed to "frequently"

3. *P2L27: What motion detector system? This has not be referenced yet.*

   We added "(see Section 2.1)", as the detection system of the MASC is described there.

4. *L28-29: How was this adapted, because Praz et al., 2017 says nothing about "blowing snow", "drifting snow", or "fragmented grains".*

   We changed "combined with" into "In addition to".

5. *P2L31-33 Unclear motivating statement.*

   We have changed into: "...extracted from pictures collected by...".

6. *P3L17 Does this mean the cameras are not synchronously taking pictures? If so, the sampling frequency is 1 Hz, a distinction of great relevance for blowing snow measurements, where counts scale with flux. This is confusing for Figure 3. What rate is maximal?*

The pictures are synchronously taken from the three cameras, at a maximum rate of 3 Hz as can be seen in Figure 6. A reference to Fig.6 has been added at the end of the sentence.

7. *P3L20: A better comprehensive reference of (blowing) snow measurement techniques is Kinar and Pomeroy (2015).*

   Thanks for the reference! We have also added it earlier in the text (3rd paragraph of the introduction).

8. *P4L5-13 Refer to the Table, and use the actual months that contained observations (8 days Nov-Jan, etc.), so as to not overstate the amount of data used. Consistently reference the dates (i.e. not just years for one data set and years and months for the other).*

   Table 1 lists the dates retained to build the training set but the actual duration of the series is much larger. We have clarified the duration of the three data sets.

9. *P4L13 Was this 11.5 days total? Please clarify.*

   We are sorry but we do not understand the question from the reviewer. We hope that the clarification above answers the question.

10. *P4L15 Choose not chose.*

    Changed.

11. *P4L15 Rephrase "enough". A sufficient number of?*

    Changed.

12. *P4L16 classes not class.*

    Changed.

13. *P4L16 Especially? How so?*

    We changed the text into:
    in particular for the Antarctic data set in which mixed images are very frequent.

14. *P4L16 Rephrase "appeared less trivial than expected".*

    We changed the text into:
    ...turned out to be more complicated than expected...

15. *P4L17 For those that study the cryosphere, but not East Antarctica, how far away are these stations, and are they similar?*

    Neumayer is on the coast while Princess Elizabeth in about 200 km in land. These stations are mentioned simply because the study by Gossart et al (2017) is using data collected there, but there is no particular importance of their locations for our study. We have added "coastal" after Neumayer and "inland" after Princess Elizabeth in the text to quickly give an idea about the different locations of those two stations.

16. *P4L19 "For the sake of generalization..." is not a sentence.*

    We changed the text into:
    For the sake of generalization, a large number of representative events was selected across the three campaigns.

17. *P4L20 Correct the phrase "hydrometeors types as well as snowfall rate".*

    We changed the text into:
    and a wide range of snowfall intensities

18. *P5L5 The sentence beginning with "Similarly" seems like an incomplete or unconnected thought.*

    We changed the text into:
    a wide range of wind speeds and concentrations

19. *P5L7-9 Why would the image frequency need to be lower than the median during pure precipitation? Is there a physical basis for that?*

    The median was chosen as a threshold to select values that are high (relatively to their respective distributions), but there is nor physical reason that the values of image frequency associated with precipitation should be below the median. This criterion on the image frequency is used in combination with a similar one for wind and no precipitation during the preceding hour. So all these criteria combined should ensure to select blowing snow. We have added after "their respective median estimated over the whole campaign":
    (to select relatively high values)

20. *P5L14-16 Please be consistent with tenses throughout the paper "we noticed...one could notice".*

    We changed "one could notice" to "we noticed" to be consistent.

21. *P5L16 Is augment the right word choice here?*

    We changed "augment" into "enlarge".

22. *P5L19-20 What is this "uncertainty?" Is this 4263 unique instances, or 1421 unique timesteps? Previously commented.*

    The uncertainty mentioned here corresponds to the uncertainty in the manual labeling of MASC images with particular types. We changed "exact" to "assigned".
    There are 4263 images (considering all cameras independently) corresponding to 1421 unique timestamps (triplets). We added (1421 triplets) after "4263 images".

23. *P7L6-7 Can you make a mention of the focal length of these cameras? i.e. are all particles always in focus? This is critical for distinguishing blowing snow particles from falling snow.*

    The focal length is 12.5 mm, but the particles are not always in focus. An empirical quality criterion is proposed in Praz et al., (2017) that can be used to automatically filter out images too much out of focus, but is not used here. The following text has been added (see Section 2.1):
    (with a focal length of 12.5 mm)

24. *P7L12 What is the window size of your median filter? Median filters have an effective smoothing, depending on window size, essentially blurring all edges.*

    This median filter is a "temporal" filter and not a spatial filter. The median image is computed over 5 consecutive images, as mentioned on l.17.

25. *P7L16 "rarely", not "hardly". "in" not "on". get rid of few or replace with multiple.*

    Changed.

26. *P7L23 Rephrase "by a too long period of time".*

    We removed "too long".

27. *P7L27 A more standard and original reference to cite for decomposition of blowing snow grains is Schmidt, 1980 "Threshold wind-speeds and elastic impact in snow transport".*

    We added the reference.

28. *P7L29 A bit more effort should be made to cite papers where these ideas originated (Budd et al., 1966 "The byrd snow drift project: outline and basic results" and Budd 1966 "The drifting of nonuniform snow particles").*

    We added the references.

29. *P8L1-3 What does that mean? Sentence starting "As..."*

    We have modified the sentence as follows:
    As the classification is performed at the image level, we need features at the same level and the information on the geometry and size of each detected particle in the considered image must hence be transformed into a single descriptor for that image.

30. *P9L3 Replace pertinent.*

    We changed to "relevant".

31. *P10L7 This choice seems awfully arbitrary. Can it be backed up by anything?*

    This choice is based on the S values obtained for different quantiles tested. It is now mentioned in the text.

32. *P10L14-15 And what is the significance of having the largest S value?*

    The distance quantified by the descriptor S (see Eq.1) is selected to rank the different possible features that can be extracted from a 2D images as MASC pictures. We therefore select the features corresponding to the highest S values (indicating that the selected features have the largest discriminative potentials).

33. *P10L17 Refers back to my original concern. How do we know all the other machinery surrounding the image frequency is necessary?*

    See our response to item 1 in the section "General Comments" above.

34. *P11L8 You mean many-fold not manifold.*

    We changed the sentence as follows:
    The choice of an unsupervised approach is based on several reasons.

35. *P12L1 Clear it up and define what the vectors are: "x=(image freq,...)".*

    We have added: ($\vec{x} = \{f_i\}, i = 1..4$, where f_i are the 4 features listed in Table 2) after "four dimensional".

36. *P12L2 "for this purpose".*

    Changed.

37. *P12L21 Rephrase "In words"*

    Changed to "That is to say".

38. *P13L6-7 Where is the degree of mixing actually verified? I only see uncertainty later on, not something physical. Refer to second major comment.*

    We do not have reference data to verify the degree of mixing (only images corresponding to mixed cases but without an estimation of this degree of mixing). See our response to item 2 in the section "General Comments" above.

39. *P13L7-8 This "likelihood" is entirely contingent on your method working. If it does not work, being near the decision boundary means inconclusive.*

    The mixed cases can only appear at the edges of the GMM peaks, here centered by construction on the two "pure" ends of the spectrum that are clearly separated in the 4-dimension space we fit the GMM in (see Fig.7 for instance). Hence the mixed cases are by construction in between the GMM peaks.
    Now the probability we derive is indeed relevant only if the fitted GMM properly describes the empirical joint distribution. We do not have reference data for mixed cases, so we cannot quantitatively evaluate this probability for the mixed cases, but the general trend (conditioned by the GMM) is expected to be correct.

40. *P13L11-13 Rephrase sentence beginning with "Nevertheless..."*

    The sentence has been modified as follows:
    In order to investigate this issue, an additional set of images corresponding to mixed cases was built: it exhibited clear differences in the posterior probabilities with the pure blowing snow and pure precipitation subsets.

41. *P15L1 Rephrase "The terms have usually opposite signs..."*

    The sentence has been rephrased as follows:
    The minus in front of the logarithm on the left side of Eq. 6 is used to return positive values...

42. *P16L5-7 Again, how was this generated?*

    The percentage values provided have been obtained by applying the proposed algorithm, once trained on the specific subsets (see Section 4.2), to the entire data sets at hand (see Section 2.2). We modified the text as follows to clarify this aspect:
    The method presented (and fitted) in the previous sections is now applied to...

43. *P16L12-13 This is not immediately clear. Precipitation particles are most clearly evident in the top subplot, whereas the blowing snow (combined with mixed?) are dominant below.* Please clarify.

    The text has been modified as follows:
    It is also clear from Figure 10 (bottom) that blowing snow and mixed blowing snow are more frequent than precipitation and mixed precipitation.

44. *Fig.10 Why is there a peak around 45 degrees? Does this not imply some tendency towards inconclusive results as the probability is neither one nor the other? I do not recall a training specifically for mixed grains.*

    This peak near 0.5 for the normalized angle is also visible in Fig.11 (Davos data set) although slightly lower (about 0.47). In addition, there is no such peak in Fig.9 (almost pure blowing snow and pure precip images). This behavior indicates in our view that this peak has a physical basis and is not a pure artifact. As we do not have (quantitative) referenced observations for mixed cases, this unfortunately remains a bit speculative...

45. *Fig 11 Are these results? What ground truth do we have for a comparison? These results seem largely qualitative.*

    Figure 11 displays the outcome of the propose classification method to the entire Davos data set, as Figure 10 does it for the entire Antarctica data set. As the performance of the method has been demonstrated to be good for pure blowing snow and pure precipitation (see Section 4.2), these figures do present results, at least for these two categories. Concerning mixed cases, the results are less quantitative because of the lack of reference data, but still relevant (as for instance the distributions are different between the two regions, in agreement with the respective climatic features) and worth showing in our view.

46. *P17L5 Reword sentence beginning with "The proposed..."*

    We modified the sentence as follows:
    Beyond global statistics on various data sets as presented above, the proposed approach can also be used to investigate the type of images at high temporal resolutions.

47. *P18L1-2 This seems to imply that you are classifying each cameras images separately. How often did the three cameras agree or disagree in the same few hundredths of a second? This comparison would help bolster the claims that the authors are coming up with self-consistent results. Furthermore, the image classifications self-consistent if one was to remove image frequency? That is, do the other image analysis metrics represent something actually physically relevant, or are the results then "noisy".*

    About the processing of the three views independently and the consistency of the outcome, this is explained on p.15 (l.25-28). The classification is indeed consistent and marginal differences appear between the three views, showing the robustness of the classification. The mention of hundredths of second was erroneous, and was changed to "a few seconds", as illustrated in Fig.12.
    Concerning the added value of the other descriptors than the image frequency, see item 1 in the General Comments above.

48. *P18L3-4 Rephrase "the type...and mixed".*

    The sentence was rephrased as follows:
    the types precipitation and mixed are dominant

49. *P18L5-6 Rephrase the sentence beginning "Finally..."*

    The sentence was changed to:
    After 22:00, mixed cases dominate and some images corresponding to precipitation are detected towards the end of the event

50. *Fig 12 Really hard to interpret. Please use a binary image or increase the contrast.*

    We have changed Fig.12 and now use the binary images.

51. *Fig 13 Interesting! And whats the actual truth here? How likely is it that there was "Pure Blowing Snow" happening concurrently with "Pure Precip"?*

    As with any classification (or model more generally), the truth is hardly known. The concurrent occurrence of blowing snow and precipitation is very likely in Dumont d'Urville, where katabatic winds are very frequent, even during precipitation (Vignon et al., 2019). This is now mentioned in the text.

52. *Fig 14 Use more obvious overlapping patterns. It is unclear what is happening when more than two distributions start overlapping.*

    We did our best but could not find a better way to figure the overlap. In addition, the regions where more than 2 distributions overlap are limited, and although not totally clear, do not hamper the interpretation of the main aspects of this figure.

53. *P20L10 Where is Davos blowing snow? If this is blown right off of the fence tops, it should look something like a mix of fresh precip and blowing snow as it has not had a chance to fragment on the ground.*

    The amount of images corresponding to pure blowing snow in Davos is very limited (0.6%, see Table 3) and deemed not representative, because of the DFIR. So we decided not to plot those as we have a lot of pure blowing snow images from Antarctica.

54. *P21L15-16 This has not been convincingly argued.*

    We have rephrased this paragraph to clarify our results.

55. *P21L18-19 This is in effect a methods paper with minimal validation. At the moment, these conclusions are suspect.*

    We understand the concern about the lack of validation data, for the mixed case only. This being said, the proposed method is thoroughly evaluated for the pure blowing snow and pure precipitation types. The text has been modified to better highlights the strengths and limitations of our approach. But we respectfully disagree with the reviewer when they state that our conclusions are all suspect.

56. *P22L1-3 Why not use the actual weather station data nearby, instead of relying on statistics from other years. This reliance makes the conclusions weaker than necessary.*

    We are not sure to get the point... The reference to Gossart et al. (2017) is used here to show consistency of our results with existing work in the Antarctic environment. And we do not see how we could use standard meteorological observations (without precipitation) to infer the respective occurrence of blowing snow and precipitation.

57. *P22L19-20 This should be mentioned much earlier, as there is no reason this assumption should hold.*

    There is no a priori reason to have the features normally distributed, but the GMM is fitted in order to best match the empirical distribution, by selectng the GMM parameters minimizing the Akaike information criterion (AIC) and the Bayesian information criterion (BIC).

Identification of blowing snow particles in images from a multi-angle snowflake camera

Mathieu Schaer[1], Christophe Praz[1], and Alexis Berne[1]

[1] Environmental Remote Sensing Laboratory, École Polytechnique Fé dérale de Lausanne, Switzerland

Correspondence: Alexis Berne (alexis.berne@epfl.ch)

Abstract. A new method to automatically discriminate between hydrometeors and blowing snow particles on Multi-Angle Snowflake Camera (MASC) images is introduced. The method uses four selected descriptors related to the image frequency, the number of particles detected per image as well as their size and geometry to classify each individual image. The classification task is achieved with a two components Gaussian Mixture Model fitted on a subset of representative images of each class from field campaigns in Antarctica and Davos, Switzerland. The performance is evaluated by ~~labelling~~ labeling the subset of images on which the model was fitted. An overall accuracy and Cohen's Kappa score of 99.4 and 98.8%, respectively, is achieved. In a second step, the probabilistic information is used to flag images composed of a mix of blowing snow particles and hydrometeors, which turns out to occur frequently. The percentage of images belonging to each class from an entire austral summer in Antarctica and during a winter in Davos, respectively, are presented. The capability to distinguish precipitation, blowing snow and a mix of those in MASC images is highly relevant to disentangle the complex interactions between wind, snowflakes and snowpack close to the surface.

1 Introduction

Over snow covered regions, ice particles can be lifted from the surface by the wind and suspended in the atmosphere. Wind-driven snow transport is ubiquitous in the cryosphere: over complex terrain (e.g. Winstral et al., 2002; Mott and Lehning, 2010), over tundra/prairies (e.g. Pomeroy and Li, 2000) and over polar ice sheets (e.g. Bintanja, 2001; Déry and Yau, 2002; Palm et al., 2011). Wind-driven snow transport must be taken into account to obtain accurate estimates of the mass balance and radiative forcings at the surface (e.g. Gallée et al., 2001; Lesins et al., 2009; Scarchilli et al., 2010; Yang et al., 2014). In mountainous regions, wind-transported snow also creates local accumulations and irregular deposits, being a critical factor influencing avalanche formation (e.g. Schweizer et al., 2003). Quantifying snow transport during snowfall events and subsequent periods of strong winds is essential for local avalanche prediction (e.g. Lehning and Fierz, 2008). In the context of climate change, the mass balance of the Antarctic ice sheet is of increasing relevance due to its impact on sea level rise (Shepherd et al., 2012). The sustained katabatic winds in Antarctica generate frequent blowing snow events, that remove a significant amount of new snow through transport and sublimation. Wind-transported snow is hence an important factor to take into account when considering Antarctic mass balance (e.g. Déry and Yau, 2002; Scarchilli et al., 2010; Lenaerts and van den Broeke, 2012; Das et al., 2013). Blowing snow is also an important process for the mass balance of the Greenland ice sheet (e.g. Box et al., 2006).

~~The layers formed by wind-suspended ice particles are commonly separated in two classes: drifting snow when the top of this layer is less than 2 m above ground, blowing snow above (see for instance). The present study focuses on blowing snow because~~ Ice particles moving at the snow surface belong to one of the three main types of associated motion: creep, saltatation and suspension (e.g. Kind, 1990). Given the fact that the observations used ~~for detection were collected more than 2 m above ground (but the proposed approach could easily be extended to drifting snow if relevant data are collected/available)~~ in the present study were collected about 3 m above the ground (or snow surface) level, the term “blowing snow" hereinafter refers to wind-suspended ice particles.

Blowing snow is challenging to measure and characterize. Various approaches have been proposed to monitor blowing snow at ground level: mechanical traps, nets, photoelectric or acoustic sensors, photographic systems ~~(see Leonard et al., 2012, for a more detaile~~ (Leonard et al., 2012; Kinar and Pomeroy, 2015). Although not specifically designed for blowing snow, present weather sensors have been shown to be valuable to monitor drifting and blowing snow fluxes (e.g. Bellot et al., 2011). Remote sensing, and lidar systems in particular, have recently been used to characterize the occurrence and depth of blowing snow layers, either from space (Palm et al., 2011) or near ground-level (Gossart et al., 2017). Suspended ice particles are under the influence of the gravitational force, proportional to the size cubed while the drag force is proportional to the area (size squared). With a greater area to mass ratio, smaller particles are thus more likely to be lifted in the suspension layer. A comparison of ten different studies of measured and simulated particle size distributions of blowing snow, reveals mean diameters at heights above $0.2\,\mathrm{m}$ ranging from 50 to $160\,\mu\mathrm{m}$ (Gordon and Taylor, 2009).

Blowing snow may also contaminate precipitation observations collected by ground-based sensors, ~~obviously~~ frequently in Antarctica (e.g. Nishimura and Nemoto, 2005; Gossart et al., 2017) where winds are strong and frequent, but also in snowy regions in general (Rasmussen et al., 2012; Naaim-Bouvet et al., 2014; Scaff et al., 2015). The issue of snowfall measurement is complex and WMO promoted intercomparison projects to evaluate various sensors and define standards set-ups and protocols over the last two decades, as illustrated in (Goodison et al., 1998) and the recent SPICE project (http://www.wmo.int/pages/prog/www/IMOP/intercomparisons/SPICE/SPICE.html).

The Multi-Angle Snowflake Camera (MASC) is a ground-based instrument designed to automatically captures high resolution ($\sim$$33.5\,\mu\mathrm{m}$) photographs of falling hydrometeors from three different angles (Garrett et al., 2012). The MASC has been used in previous studies to investigate snowflake properties (Garrett et al., 2015; Grazioli et al., 2017) and to help interpret weather radar measurements (Kennedy et al., 2018). Interestingly, blowing snow particles also trigger the MASC motion detector system (see Section 2.1), producing many images in windy environments. ~~Combined with the~~ In addition to hydrometeor classification techniques based on MASC images (e.g. Praz et al., 2017), the ability to discriminate between images composed of blowing snow and precipitation particles ~~is therefore~~ would therefore be relevant to characterize blowing snow, to provide reference observations to improve its remote sensing, as well as to obtain more accurate snowfall estimates from ground-based sensors. More generally, detailed information about the type of particles ~~pictured~~ extracted from pictures collected by a MASC will enable us to further investigate the complex interactions between wind, snowflakes and snowpack close to the surface in cold and windy regions.

This article presents a new method to automatically determine if an image from the MASC (and potentially other imaging instruments) is composed of blowing snow particles, precipitating hydrometeors (snowflakes and ice crystals) or a mix of both. The classification is accomplished by means of a Gaussian mixture model (GMM) with two components, fitted on a set of representative MASC images and evaluated on a manually-built validation set. The paper is organized as follows: Section 2 introduces the data sets used to develop the method and fit the GMM. Section 3 illustrates the different steps to isolate the particles and extract related features for the clustering task. Section 4 explains the selection of the most relevant features, the fitting of the GMM as well as the attribution of a flag for mixed images. The main results are shown in Section 5. At last, limitations and further improvements are discussed in Section 6.

2 Instrument and data sets

2.1 The Multi-Angle Snowflake Camera

The MASC is a ground-based instrument which automatically takes high-resolution and stereoscopic photographs of hydrometeors in free fall while measuring their fall velocity. Its working mechanism is only summarized hereafter, as more details and explanations can be found in Garrett et al. (2012), who provide an extensive description of the instrument. Three high-resolution cameras (2448 × 2048 pixels), separated by an angle of 36°, are attached to a ring structure and form altogether the imaging unit (see Fig. 1). The focal point is located inside the ring at about $10\,\mathrm{cm}$ from each camera (with a focal length of 12.5 mm). Particles falling through the ring and detected by the two horizontally aligned near-infrared emitter-receiver arrays trigger the three flashes and the three cameras. The cameras' apertures and exposure times were adjusted in order to maximize the contrast on hydrometeor photographs while preventing motion blur effects, leading to a resolution of about $33.5\,\mu\mathrm{m}$ and a sampling area of about $8.3\,\mathrm{cm}^2$ (see Praz et al., 2017). The maximum frequency of triggering is $3\,\mathrm{Hz}$, that is three image triplets per second (see Fig. 6).

These specifications can be compared to the snow particle counter (SPC) which has been used in many studies of blowing snow ~~(e.g. Nishimura and Nemoto, 2005; Gordon and Taylor, 2009; Guyomarc'h et al., 2019)~~ (e.g. Nishimura and Nemoto, 2005; Gordon and can be considered as the reference instrument for monitoring blowing snow (e.g. Crivelli et al., 2016). The SPC has a control volume of $2 \times 25 \times 0.5\,\mathrm{mm}^3$ and assigns particles into 32 diameter classes between 50 and $500\,\mu\mathrm{m}$. It provides information on particle diameter (assuming a spherical shape), particle number and particle mass flux usually at a 1-s resolution (but raw data are measured at up to 150 kHz, Nishimura et al., 2014). For more information about the SPC, the reader is referred to the articles mentioned above.

Figure 1. Left: side-view of the MASC with the three flash lamps in white on top, the two detectors as white boxes on the side of the metal ring (in black and red in front). Right: top view of the inside of the MASC, with the three cameras clearly visible.

2.2 Data sets

The MASC data used to implement and validate the present algorithm were collected during three field campaigns. The first one took place in Davos, Switzerland ~~during the winter 2015-2016.~~ from October 2015 to June 2016. The MASC was placed at $2540\,\mathrm{m}$ a.s.l in a Double Fence Intercomparison Reference (DFIR, see Fig. 2, left), designed to limit the adverse effect of wind on the measuring instruments in its center (Goodison et al., 1998). The MASC was about $3\,\mathrm{m}$ above ground. The two other campaigns took place at the French Antarctic Dumont d'Urville station, on the coast of Adelie Land, ~~during the austral summer 2015-2016~~ from November 2015 to February 2015 and from January to July 2017 in the framework of the Antarctic Precipitation, Remote Sensing from Surface and Space project[1] (Grazioli et al., 2017; Genthon et al., 2018). The instrument was deployed on a rooftop at about $3\,\mathrm{m}$ above ground (see Fig. 2, right). A collocated weather station and a micro rain radar (MRR) were also installed. Nearly three millions images were collected during these measurement campaigns all together.

From this great amount of data, subsets of pure precipitation and pure blowing snow images were manually selected and further analyzed to ~~chose~~ choose relevant descriptors and fit a two components GMM. The task of selecting ~~enough representative images from both class appeared less trivial~~ a sufficient number of representative images for both classes turned out to be more complicated than expected, ~~especially for Antarctica, as~~ in particular for the Antarctic data set in which mixed images are ~~especially common~~very frequent. Gossart et al. (2017) used ceilometer data collected at the Neumayer (coastal) and Princess Elizabeth (inland) stations in East Antarctica to investigate blowing snow, and they suggests that more than 90% of blowing snow occurs during synoptic events, usually combined with precipitation. For the sake of generalization, ~~as many representative events as possible were~~ a large number of representative events was selected across the three campaigns. The goal was to cover a wide range of hydrometeors types ~~as well as snowfall rate~~ and a wide range of snowfall intensities for the precipitation subset. Similarly, ~~varying~~ a wide range of wind speeds and ~~concentration densities~~ concentrations were considered to build

[1] http://apres3.osug.fr

Figure 2. Experimental set-up conditions of the MASC in a DFIR near Davos (left) and on top of a container at Dumont d'Urville (right).

the blowing snow subset. From the campaigns in Antarctica, pure blowing snow and hydrometeors events were highlighted by comparing time series of MASC image frequency, wind speed and MRR derived rain rate, as illustrated in Figure 3. It was noticed that during strong blowing snow events, the number of images captured by the MASC was much larger than during precipitation events (more than 1 image per second, see Fig. 6). Potential pure blowing snow events were selected when the MASC image frequency and wind speed were higher than their respective median ~~observed~~ estimated over the whole campaign (to select relatively high values) and no precipitation was detected during the preceding hour. Only events for which these criteria applied for over an hour consecutively were kept. To highlight pure precipitation, the principle was the same but the criteria were an image frequency and a wind speed lower than the median and a MRR precipitation rate greater than zero. The MRR has a certain detection limit, so it was noticed that events selected as blowing snow could also occur during undetected light precipitation. As a result, images from all events were rapidly checked visually and the campaign logbook consulted to ensure that the selection was consistent and coherent. In both cases, some events had to be removed because of obvious mixing of blowing snow and hydrometeors.

As the MASC was deployed inside a DFIR in Davos, no blowing snow events were selected from this campaign. Although the DFIR is supposed to shelter the inner instruments from wind disturbances, we noticed that many images do not solely contain pure hydrometeors. From a webcam monitoring the instrumental set up, ~~one could notice~~ we noticed that the fresh snow accumulated on the edges and borders of the wooden structure of the DFIR was frequently blown away towards the sensor. To ~~augment~~ enlarge the precipitation subset, events with high snowfall rate but not affected by outliers of fresh wind-blown snow were added. Finally, some sparse images of obvious pure hydrometeor in the middle of mixed events were also included in the training set. In total, each subset contained 4263 images and despite possible remaining (limited) uncertainty in the exact type of images, is assumed to be accurate and reliable enough to serve as reference for the evaluation of the proposed technique (see Fig. 8 and Section 4.2).

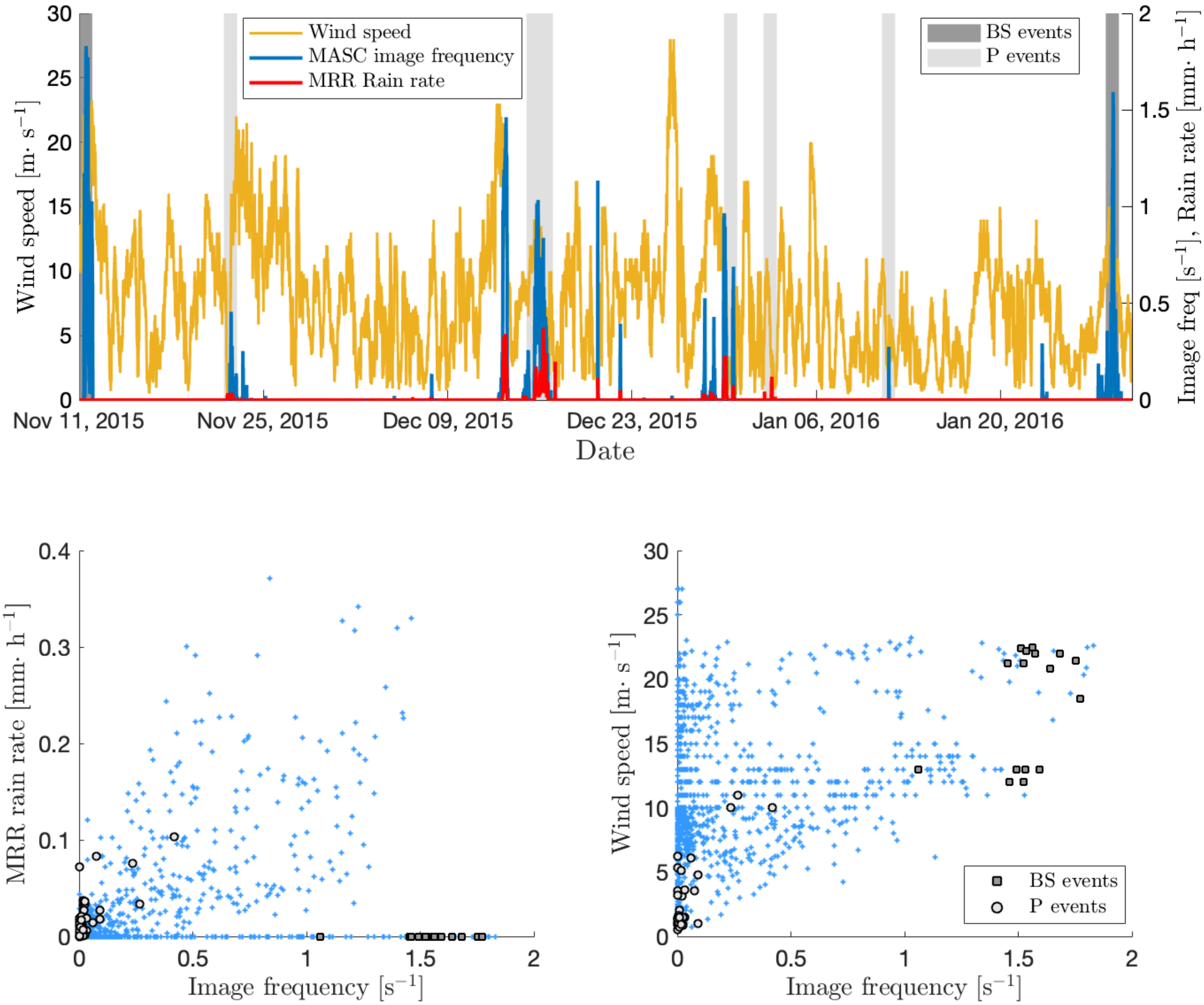

Figure 3. Time series and scatter plots of MASC image frequency, wind speed (measured at 10 m) and MRR derived rain rate for the Antarctica 2015-2016 campaign. The grey shading indicates days during which time steps have been selected for the training set as blowing snow (dark grey) or precipitation (light grey). In the bottom scatter plots, the markers figure the selected blowing snow and precipitation time steps. Points on the x-axis in the left scatter plot are potential candidates for pure blowing snow.

Table 1. Campaigns and dates of selected events for the Blowing snow (BS) and Precipitation (P) subsets.

Antarctica 15-16	**Antarctica 17**	**Davos 15-16**
11 Nov BS	08 Feb BS	23 Feb P
22 Nov P	09 Feb BS	25 Feb P
15 Dec P	18 Feb BS	04 Mar P
16 Dec P	19 Feb BS	05 Mar P
30 Dec P		16 Mar P
02 Jan P		25 Mar P
11 Jan P		
28 Jan BS		

3 Image Processing

3.1 Particle detection

~~The MASC consists of three cameras mounted on a ring structure with an angle of 36° between them and sharing the same focal point in the middle of the ring. The motion detector system is composed of two horizontally aligned near-infrared emitter-receiver arrays, which delimit a $8.3\ \mathrm{cm}^2$ detection surface in the center of the structure, where the two beams overlap (see Garrett et a . A particle passing through this area triggers the cameras together with three spotlights that illuminate the target. In the present study, all images have a size of 2448×2048 pixels.~~

The MASC instrument and the collected images are described in Section 2.1. Although a single particle activates the cameras, many MASC pictures contain multiple particles distributed over the entire image, especially when blowing snow occurs. In fact, the number of particles appearing on a single image is a key characteristic to distinguish between precipitation and blowing snow. As a result, it was deemed essential to detect all particles in each image rather than the triggering one only (which is sometimes unidentifiable). A key challenge of this approach was to get rid of the noisy background. For this purpose, a median filter was used. The brightness of the background strongly depends on the luminosity at the instant of the picture, which varies according to the time of day and can change abruptly in partly cloudy conditions when the sun suddenly appears from behind a cloud. As a result, the median filter shows better performance to remove the background when systematically re-computed over a small number of consecutive images. Assuming that snow particles ~~hardly~~ rarely appear at the exact same position ~~on few~~ in several consecutive images, the median filter was chosen to be computed over blocks of 5 images per camera angle. To ensure complete removal of the background when its brightness is greater that the corresponding median, a factor of 1.1 was applied to the filter. Finally, as some limited residual noise can still remain in the filtered image, a small detection threshold of 0.02 grayscale intensity was applied to isolate the snow particles. Masks of the sky and reflecting parts of the background (i.e. metallic plates etc) were created for each camera. The multiplication factor and detection threshold are increased in the regions delineated by the masks if the normal filtering leads locally to more pixels detected that one can expect from real particles.

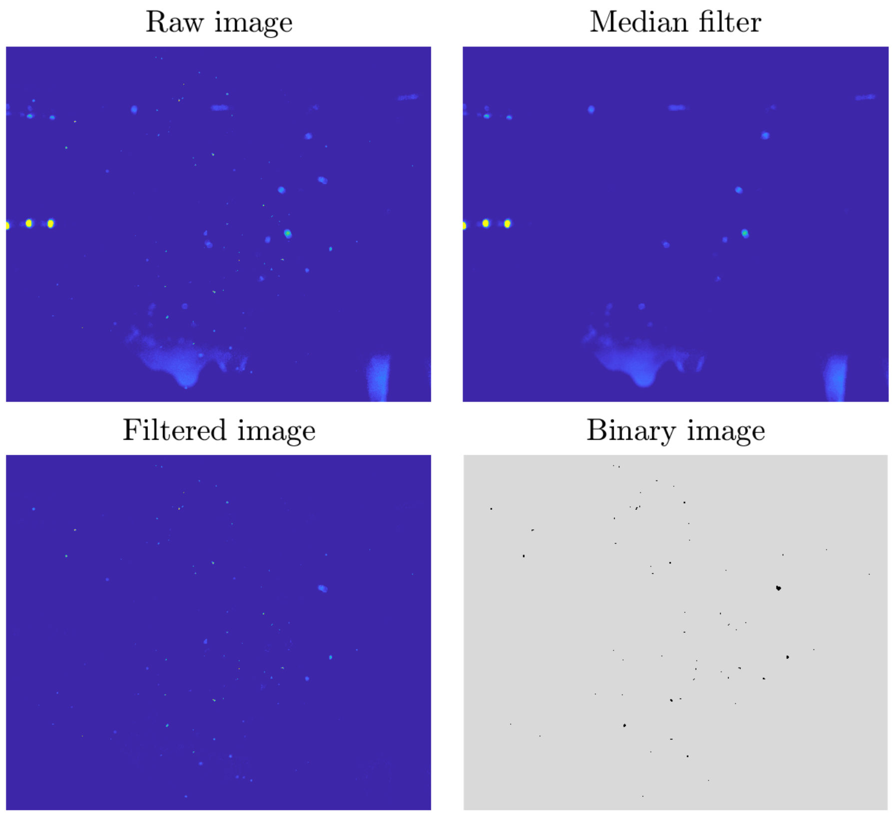

Figure 4. Raw image, median filter, filtered image and final binary image for an example of blowing snow particles. The image size is 2448×2048 pixels, corresponding to $82 \times 68.6\,\mathrm{mm}^2$. Original MASC images are in grey shades, but the color scheme used here aims to enhance contrast and details for visual purposes.

These steps are illustrated in Figures 4 and 5. Issues in the filtering may occur if consecutive images are separated by a ~~too long~~ period of time ~~,~~ during which the ambient luminosity has changed significantly (e.g. before/after the sunrise or sunset). An example is shown in Figure B1 in Appendix B.

3.2 Feature extraction

Machine learning algorithms require a set of variables, commonly called features or descriptors, upon which the classification is performed. Because of the fragmentation of ice crystals when hitting the ~~ground surface (e.g. Comola et al., 2017)~~ snow surface (e.g. Schmidt, 1980; Comola et al., 2017), blowing snow is expected to be characterized by much smaller particle size and much higher particle concentration than snowfall ~~(e.g. Nishimura and Nemoto, 2005; Naaim-Bouvet et al., 2014)~~ (e.g. Budd, 1966; Budd et al., 1966; Nishimura and Nemoto, 2005; Naaim-Bouvet et al., 2014). In this study, various quantitative descriptors were therefore calculated according to four different categories: the number of particles and their spread across the image, the size of the particles, the geometry of the particles and the frequency at which the images are taken.

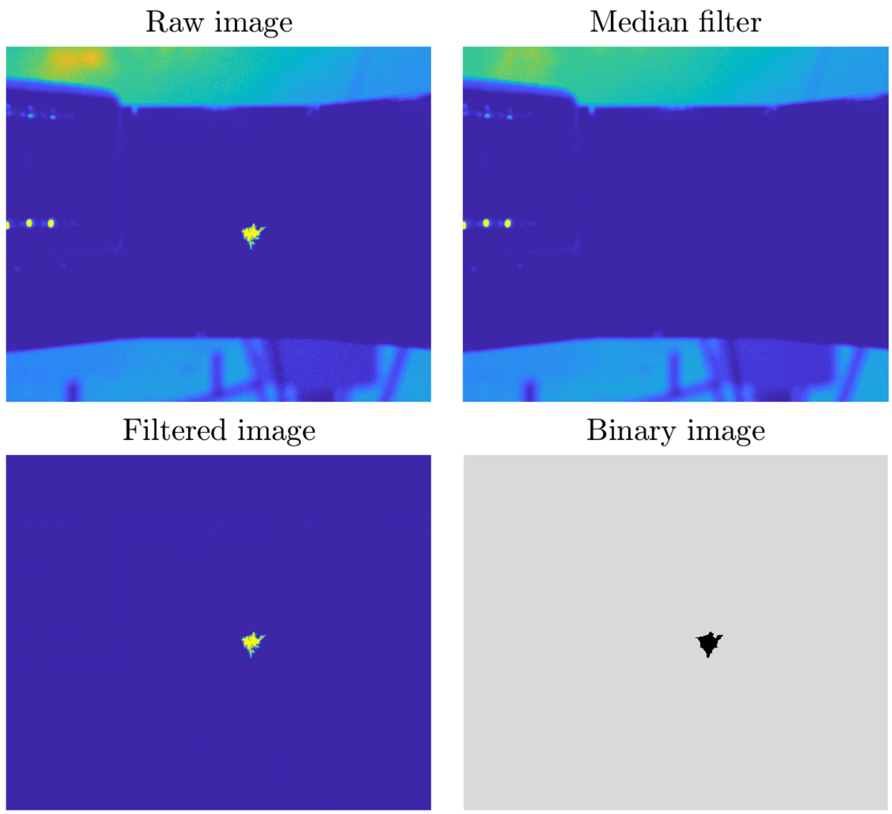

Figure 5. Raw image, median filter, filtered image and final binary image for an example of hydrometeor. The color scheme is used to enhance details for visual purposes.

Since it is difficult to exactly guess which descriptors are the most adequate to differentiate between blowing snow and precipitation images, an extensive collection of features was extracted from the blowing snow and precipitation subsets and compared. The selection of the most relevant ones is explained in the next section. As the classification is performed at the image level, we need features at the same level and the information on the geometry and size of each detected particle in the ~~image was~~ considered image must hence be transformed into a single descriptor for that image. Consequently, quantiles ranging from 0 to 1 and moments from 1 to 10 were computed out of the distribution of the considered feature within the image. The image frequency is a descriptor independent from the content of the image and thus from the detection of particles. It is therefore not affected by potential image processing issues. As each image comes with its attributed timestamp, the average number of images per minute was calculated with a moving window. The full list of all computed descriptors is displayed in Appendix A. The extraction of features was conducted with the `MATLAB` Image Processing Toolbox, in particular the function `regionprops`[2].

[2] https://ch.mathworks.com/help/images/ref/regionprops.html

4 Classification

4.1 Feature selection and transformation

Selecting a ~~pertinent~~ relevant set of features and avoiding redundancy is essential for accurate classification, regardless of the classification algorithm. For each of the four categories of descriptors previously mentioned, the most relevant one (according to the criterion explained below) was kept. The descriptor maximizing the "inter-clusters over intra-clusters" distance described in Eq. 1 was selected. This quantity represents the distance between the mean of the blowing snow and precipitation distributions (μ_{BS} and μ_P respectively), normalized by the sum of their respective standard deviations (σ_{BS} and σ_P respectively).

$$S = \frac{|\mu_{BS} - \mu_P|}{\frac{1}{2}(\sigma_{BS} + \sigma_P)}. \tag{1}$$

For the features describing the number of detected particles and their spread across the image, the *cumulative distance transform* was kept. It represents the sum over each entry of the distance transform matrix[3] of the binary image. The distance transform matrix has the same dimensions as the binary image and computes, for each pixel, the Euclidean distance to the nearest 1 element (i.e. the nearest particle). As a result, an image with many particles well distributed over its entire surface will have a low *cumulative distance transform*, while a single particle, even particularly large, will have a high value. This descriptor is more robust to image processing issues than the raw number of particles, as illustrated in Figure B2 in Appendix B.

Concerning the size distribution of the particles detected in an image, the quantile 0.7 of the maximum diameter was selected (because it has the highest S value among the different quantiles tested). The maximum diameter (*Dmax*) represents the longest segment between two edges of a particle (see Praz et al., 2017, for more details). A logarithmic transformation of this feature was performed to make the distributions of the two classes more Gaussian. The minimum (i.e. quantile 0) squared fractal index showed the greatest S value (hence discrimination potential) among the features related to the particle geometry indices. The fractal index (FRAC) is defined according to the formula proposed by McGarigal and Marks (1995) in the context of landscape-pattern analysis. It was also more recently used to quantify stand structural complexity from terrestrial laser scans of forests (Ehbrecht et al., 2017).

Due to its different nature, the image frequency descriptor was selected by default, but it is worth noting that it has the highest S value (Eq. 1) among all descriptors (Table 2). The marginal distributions of the selected descriptors for the training set are shown in Figure 6 to provide an idea of their respective magnitude and variability, as well as to illustrate their discrimination potential. As noted above, the image frequency is the most informative descriptor to distinguish blowing snow and precipitation.

In summary, four descriptor categories (related to particle size, particle geometry and particle distribution within the image as well as image frequency) have been defined to distinguish images collected during blowing snow or snowfall, based on the expected differences in particle size and concentration between the two. A number of descriptors were estimated from each image by computing various quantiles and moments of the distributions of geometric properties of the particles in the

[3] https://ch.mathworks.com/help/images/ref/bwdist.html

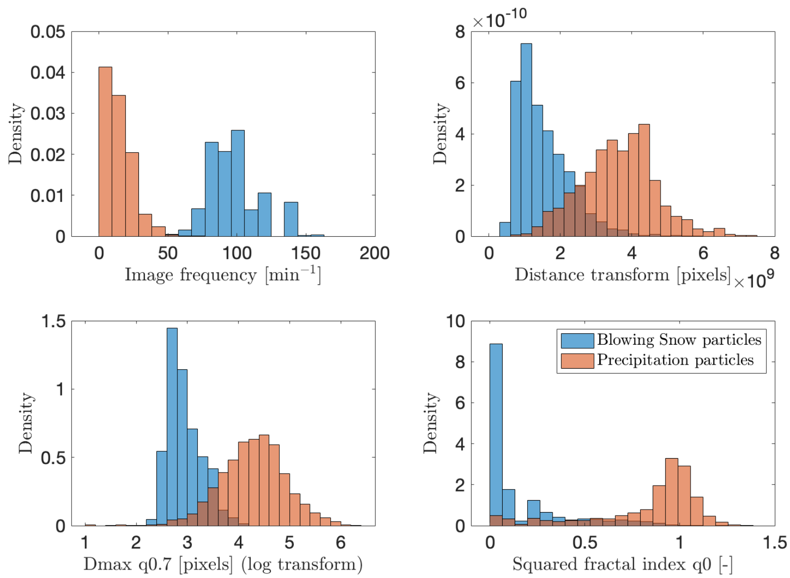

Figure 6. Histograms of selected descriptors for the training blowing snow and precipitation subsets.

Table 2. Selected features and corresponding S values

Feature name	S
Image frequency	4.43
Cumulative distance transform	2.89
Maximum diameter quantile 0.7	1.71
Squared fractal index quantile 0	3.81

considered image. One descriptor from each of the four categories defined above (listed in Table 2) was then selected to be further used for classification as the one maximizing the “inter-clusters over intra-clusters" distance defined in Eq. 1.

4.2 Model fitting

The choice for the binary classification task was made on a Gaussian mixture model, an unsupervised learning technique that fits a mixture of multivariate Gaussian distributions to the data (see Murphy, 2012; McLachlan and Basford, 1988; Moerland, 2000, for more details). The mathematical description of a multivariate normal distribution is provided in Eq. 2.

$$\mathcal{N}(\boldsymbol{x}|\boldsymbol{\mu},\boldsymbol{\Sigma}) = \frac{1}{(2\pi)^{D/2}|\boldsymbol{\Sigma}|^{1/2}} \exp\{-\frac{1}{2}(\boldsymbol{x}-\boldsymbol{\mu})^T\boldsymbol{\Sigma}^{-1}(\boldsymbol{x}-\boldsymbol{\mu})\}. \tag{2}$$

where $\boldsymbol{x}$ is a Gaussian multivariate random variable of dimension D, $\boldsymbol{\mu}$ its mean and $\boldsymbol{\Sigma}$ its covariance matrix, with ^{T} the transpose operator.

The ~~justification for the~~ choice of an unsupervised approach is ~~manifold~~based on several reasons. First, unsupervised methods do not depend upon labels. Hence, it is not required to ensure correct ~~labelling~~ labeling of each image in the training set. As mentioned earlier, many images are composed of mix of blowing snow and precipitation and it is thus difficult to guarantee the objectivity of all given labels. Second, a clear separation observed between the two subsets would be statistically highly significant as no prior information is provided to the learning algorithm about the classes. Third, for low dimensional problems, unsupervised methods are sometimes less prone to over-fitting and have a better potential of generalization. A main advantage of the GMM compared to other unsupervised methods is to provide posterior probabilities on the cluster assignments and thus allow for soft clustering (i.e. probabilistic assignment). In the context of the present study, this is absolutely relevant as there exists a whole continuum of in-between cases of mixed images. It should be noted that the descriptors were selected using a reference set (see previous section), but the clustering conducted by means of the GMM is itself unsupervised.

A two components GMM with unshared full covariance matrices was thus fitted to the four dimensional ($\boldsymbol{x} = \{f_i\}, i = 1..4$, where f_i are the 4 features listed in Table 2) data composed of the blowing snow and precipitation subsets. The `MATLAB` Statistics and Machine Learning Toolbox was used ~~to~~ for this purpose and the model parameters were estimated by maximum likelihood via the Expectation-Maximization (EM) algorithm[4]. The features were standardized before fitting the model. The mixing weights (or component proportions) were artificially set to 0.5 by randomly removing 80 data points from the training set and fitting again the GMM to have perfectly balanced classes. This step is essential as the model will then be used to classify new images (possibly from other campaigns). There are no reasons to give more weight to one component, as the relative proportion of blowing snow and precipitation images strongly depends on the campaign location. The posterior probabilities are computed using Bayes rule (Murphy, 2012):

$$P(z_i = k|\boldsymbol{x}_i, \boldsymbol{\theta}) = \frac{P(\boldsymbol{x}_i|z_i = k, \boldsymbol{\theta})P(z_i = k|\boldsymbol{\theta})}{P(\boldsymbol{x}_i|\boldsymbol{\theta})}, \tag{3}$$

where z_i is a discrete latent variable taking the values $1,...,K$ and ~~labelling~~ labeling the K Gaussian components. $P(z_i = k|\boldsymbol{x}_i, \boldsymbol{\theta})$ is the posterior probability that point i belongs to cluster k (also known as the "responsibility" of cluster k for point i). $P(\boldsymbol{x}_i|z_i = k, \boldsymbol{\theta})$ corresponds to the density of component k at point i (i.e. $\mathcal{N}(\boldsymbol{x}_i|\boldsymbol{\mu}_k, \boldsymbol{\Sigma}_k)$) and $P(z_i = k|\boldsymbol{\theta})$ represents the mixing weight (also denoted π_k). Note that the π_k are positive and sum to 1. $\boldsymbol{\theta}$ refers to the fitted parameters of the mixture model $\{\boldsymbol{\mu}_1,...,\boldsymbol{\mu}_k,\boldsymbol{\Sigma}_1,...,\boldsymbol{\Sigma}_K,\pi_1,...,\pi_K\}$. $P(\boldsymbol{x}_i|\boldsymbol{\theta})$ is the marginal probability at point i, which is simply the weighted sum of all component densities:

$$P(\boldsymbol{x}_i|\boldsymbol{\theta}) = \sum_{k=1}^{K} \pi_k \mathcal{N}(\boldsymbol{x}_i|\boldsymbol{\mu}_k, \boldsymbol{\Sigma}_k). \tag{4}$$

As the concern of this study is on two components only, a more compact notation will be used for the rest of the article. The latent variable z will be replaced by k_P and k_{BS} to refer to the precipitation and blowing snow clusters, respectively. The term $\boldsymbol{\theta}$, that denotes the model parameters, will be left implicit. Assuming we are at first interested by performing some

[4] https://ch.mathworks.com/help/stats/gaussian-mixture-models-2.html

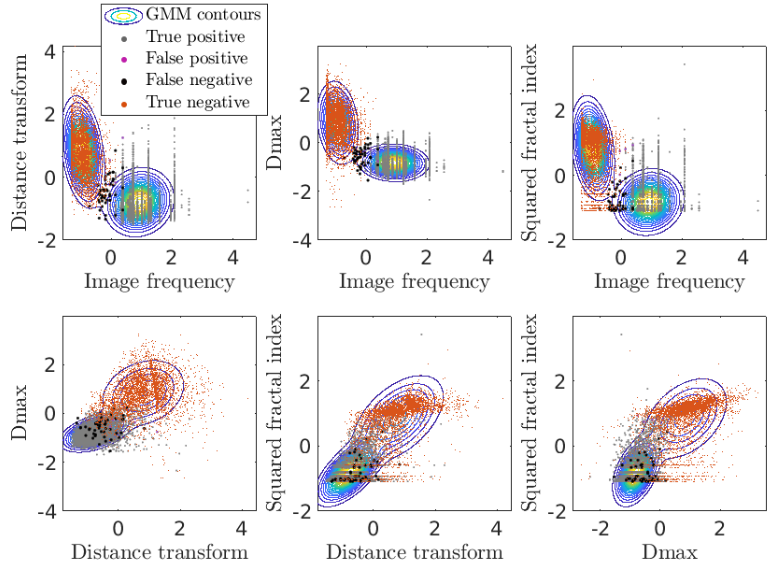

Figure 7. GMM contours and data points projected on the 2D planes. The colors correspond to the four entries of the confusion matrix. The predictions result from the clustering and the ground truth is the given labels.

hard clustering (i.e. single label to a given image), an image will be classified as blowing snow if $P(k_{BS}|\boldsymbol{x}_i) > P(k_P|\boldsymbol{x}_i)$. ~~In words~~That is to say, if the posterior probability to belong to the blowing snow cluster is greater than 0.5, an image will be classified as such (because the posterior probabilities sum to 1). The model performance was assessed by simply ~~labelling~~ labeling the data points according to its initial subset. An overall accuracy of 99.4% and a Cohen's Kappa score of 98.8% were achieved. The Cohen's Kappa statistic adjusts the accuracy by accounting for correct predictions occurring by chance (Byrt et al., 1993). These high values indicate a very good performance of the fitted GMM. Figure 7 presents the fitted Gaussian components as well as the reference values (not used in the fitting) for each of the 6 possible pairs of the 4 descriptors. It clearly illustrates the performance of the fitted GMM and the discriminative power of the descriptor related to image frequency.

To investigate the stability of the Gaussian components, the precipitation and blowing snow subsets were both randomly permuted and divided in ten equal parts. Ten new training sets of balanced amount of each subset were created and new GMM fitted. Figure 8 shows on the top line the boxplots of the Gaussian components parameters $\boldsymbol{\mu}_d$ and $\boldsymbol{\sigma}_d$ (i.e. diagonal entries of $\boldsymbol{\Sigma}$) for each of the four dimensions. The boxplots show a limited variability for each feature (below 10%), indicating a reasonable stability of the fitted parameters. In addition, the bottom line of Figure 8 presents the learning curves, and their fast convergence to the same horizontal line when more than 30% of the training set is used, indicates a data set large enough for a reliable fitting of the GMM, without overfitting.

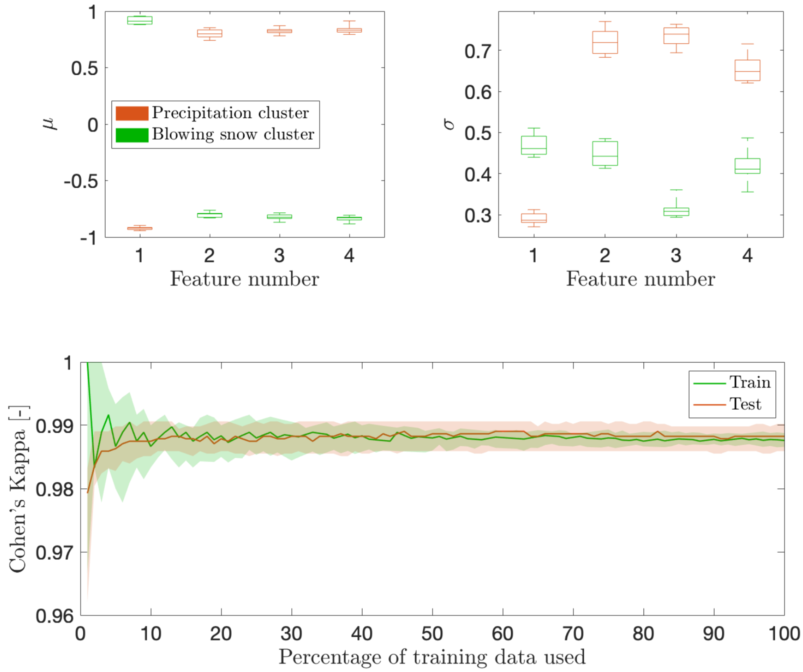

Figure 8. Top: stability of the parameters μ and σ (diagonal entries of $\mathbf{\Sigma}$) for the two Gaussian components. The boxplots show the distributions of these parameters for each dimension, after fitting the GMM on a 10-fold random split of the training set. The feature number follows the order given in Table 2. Bottom: learning curves for the fitted GMM, showing the evolution of the train and test Cohen's kappa as a function of the proportion of the training samples used. The shaded areas correspond to the 25–75 percentile range computed over 40 iterations of 70-30% random train-test splitting and bold lines are the medians.

4.3 Flag for mixed images

As mentioned earlier, an asset of using a GMM model is the posterior probabilistic information that could help estimate the degree of mixing of an image. Data points located close to the decision boundary in the multidimensional space are likely to be composed of a mix of blowing snow particles and hydrometeors. However, distributions of posterior probabilities computed over thousands of new images from entire campaigns, ~~showed that they were~~ appeared to be stretched out on both end of the domain (i.e. close to 0 or 1) and not many images were present in between. This is probably due to the nature of the descriptors and the resulting shapes and relative positions of the Gaussian distributions. ~~Nevertheless, a subset of mixed images , specially created for this purpose, highlighted clear discrepancies on~~ In order to investigate this issue, an additional set of images corresponding to mixed cases was built: it exhibited clear differences in the posterior probabilities with the pure blowing snow and pure precipitation subsets. ~~However, this differentiation was~~ This differentiation was however around 10^{-6} (or $1 - 10^{-6}$), which is not so informative as such. Consequently, it was decided to define a new index, similar to the posterior probability to belong to the blowing snow component, but more evenly distributed across the range $]0,1[$. The new index uses the negative logarithm of the posterior probabilities multiplied by the marginal probability. Taking the log of Eq.3 for k_{BS}, we have (the same applies for k_P):

$$-\log[P(k_{BS}|\boldsymbol{x}_i)P(\boldsymbol{x}_i)] = -\log[P(\boldsymbol{x}_i|k_{BS})P(k_{BS})]. \tag{5}$$

Noting that the term $P(\boldsymbol{x}_i|k_{BS})$ on the right hand side is $\mathcal{N}(\boldsymbol{x}_i|\boldsymbol{\mu}_{BS},\boldsymbol{\Sigma}_{BS})$, one can substitute Eq. 2 into the above expression, which yields:

$$-\log[P(k_{BS}|\boldsymbol{x}_i)] - \log[P(\boldsymbol{x}_i)] = \frac{1}{2}(\boldsymbol{x}_i - \mu_{BS})^T \boldsymbol{\Sigma}_{BS}^{-1}(\boldsymbol{x}_i - \mu_{BS}) + \frac{1}{2}\log(|\boldsymbol{\Sigma}_{BS}|) + \frac{D}{2}\log(2\pi) - \log(P(k_{BS})). \tag{6}$$

The quadratic term on the right hand side is the Mahalanobis Distance, which is a distance that uses a Σ^{-1} norm. Hence, it represents the distance between point $\boldsymbol{x}_i$ and the center of the distribution, corrected for correlations and unequal variances in the feature space (De Maesschalck et al., 2000). The second term is related to the determinant of the covariance matrix and equals -3.94 for the Blowing Snow component and -2.59 for the Precipitation one. The two last terms are constant and sum to 4.37 (the component proportions were set to 0.5 and $D = 4$). The right side of Eq. 6 is also known as the quadratic discriminant function (QDF, Kimura et al., 1987), commonly noted $g_k(\boldsymbol{x}_i)$. ~~The terms have usually opposite signs, but the~~ The minus in front of the logarithm ~~in~~ on the left side of Eq. 6 is used ~~here~~ to return positive values and facilitate subsequent graphical interpretations. Note that the constant term $\frac{D}{2}\log(2\pi)$ is often removed, but in this case, it ensures that $g_k(\boldsymbol{x})$ is positive, even for a Mahalanobis distance of zero. Figure 9 displays a scatter plot of the quadratic discriminant values of both components for the whole training set. The proposed index is defined as the angle of the vector representing a data point on the scatter plot, normalized by $\frac{\pi}{2}$. It is thus computed as follows:

$$\psi = \frac{2}{\pi}\arctan\left\{\frac{-\log[P(k_P|\boldsymbol{x}_i)P(\boldsymbol{x}_i)]}{-\log[P(k_{BS}|\boldsymbol{x}_i)P(\boldsymbol{x}_i)]}\right\}. \tag{7}$$

This normalized angle is bounded in $]0,1[$, with values close to 1 (respectively 0) indicating a strong membership of the considered image (and not the respective proportions within this image) to the Blowing Snow (respectively Precipitation) clusters. It is closely related to the asymmetry of the Mahalanobis distances between a point $\boldsymbol{x}_i$ and the centers of the two Gaussian distributions, but corrected by the term $\frac{1}{2}\log(|\Sigma|)$ which is different for the two components. The advantage of using the index in this form, rather than deriving it from the Mahalanobis distances alone, is to respect the decision boundary given by the maximum a posteriori (MAP) rule. This means, a posterior probability of 0.5 yields a ψ index of 0.5. Finally, quantiles 0.9 ($\psi_{P0.9}$) and 0.1 ($\psi_{BS0.1}$) of the ψ index distributions of the points classified as Precipitation and Blowing Snow, respectively, are retained as thresholds to flag potential mixed images. The idea is to allow, for both classes, 10% of the training set images being flagged as mixed. This value is qualitatively supported by the distribution shown in Figure 9. It can be changed by the user to be more (increasing it) or less (decreasing it) strict on the classification as pure blowing snow or pure precipitation, depending on the intended application.

To provide the user of the method with an easily readable output, a mixing index λ_m is introduced by linearly rescaling between 0 and 1 the ψ index of the images flagged as mixed (i.e. λ_m is not defined for pure precipitation or pure blowing snow images):

$$\lambda_m = \frac{0.5}{0.5-\psi_{P0.9}}(\psi-\psi_{P0.9}) \quad \text{if } \psi \in (\psi_{P0.9}, 0.5)$$
$$= \frac{0.5}{0.5-\psi_{BS0.1}}((1-\psi_{BS0.1})-\psi) \quad \text{if } \psi \in [0.5, \psi_{BS0.1}) \tag{8}$$

The mixing index also respects the hard clustering assignment boundary at 0.5: $\lambda_m > 0.5$ indicates that the image contains a mix of blowing snow and precipitation particles, but overall being closer to blowing snow and vice versa. Images with a normalized angle outside the two mixed thresholds have a NaN index of mixing and are considered as pure blowing snow particles or pure hydrometeors. Results are provided treating all images independently, but the ψ index can also be averaged among the three camera angles to provide a unique value per image identifier as well. The median of the range (max - min) covered by the ψ values from the three individual views is about 0.08 in Davos and 0.05 at Dumont d'Urville, indicating a limited variability between the three views.

In summary, the classification as mixed case is based on the angle characterizing the considered MASC image in the 2D space formed by the axis related to pure blowing snow on the one hand and the one related to pure precipitation on the other hand. A mixing index λ_m is finally computed by linearly rescaling the normalized angle over the range of values corresponding to mixed cases.

5 Results

The method presented (and fitted) in the previous sections is now ~~tested on~~ applied to the entire Antarctica 17 campaign (January - July 2017) and ~~on~~ to the entire Davos campaign (December 2015 - March 2016). About $2 \cdot 10^6$ images for Antarctica and $8.5 \cdot 10^5$ for Davos were classified. Table 3 summarized the outcome in terms of respective proportions of pure blowing snow, pure precipitation, mixed blowing snow and mixed precipitation, for the Antarctic and Alpine data sets. As expected, the occurrence of blowing snow (pure + mixed) is much more frequent at Dumont d'Urville (75.6%) than at Davos (21.5%, out of which only 0.6% of pure blowing snow).

Table 3. Percentages of MASC images per category

Class	Antarctica (Jan - Jul 2017)	Davos (Dec 2015 - Mar 2016)
Pure Blowing snow	36.5%	0.6%
Pure Precipitation	7.2%	39.2%
Mixed Blowing snow	39.1%	20.9%
Mixed Precipitation	17.2%	39.3%

Figure 10 shows (top) the distribution of the collected MASC images in the space formed by the two quadratic discriminant (one for blowing snow, one for precipitation) as well as (bottom) the distribution of the normalized angle for the entire Antarctica 17 campaign. A clear difference with Figure 9 is the large proportion of values corresponding to mixed cases: there are

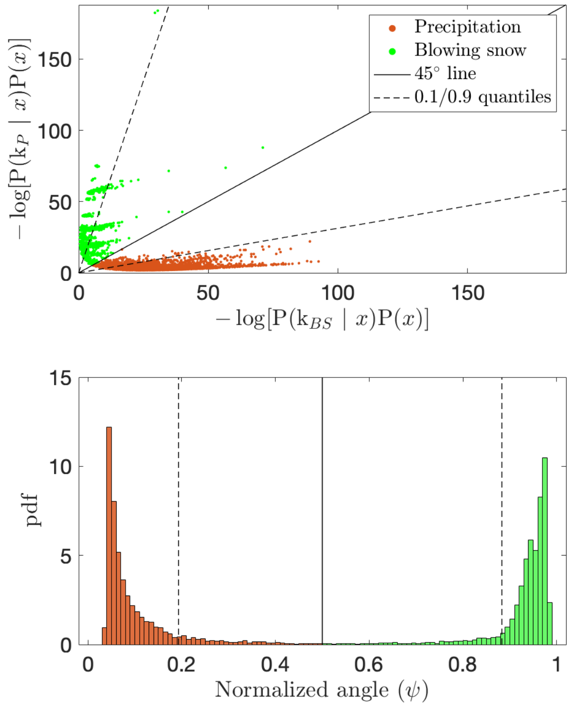

Figure 9. Top: scatter plot of the quadratic discriminant values of both components for the training set. **Bottom**: distributions of the normalized angle for the precipitation and blowing snow subsets and thresholds to identify mixed images

much more points around the one-one line (top) and a small mode around 0.5 (bottom) for the entire campaign than for the training set (built with much less mixed cases). It is also clear from Figure 10 (bottom) that blowing snow and mixed ~~cases are dominant with respect to~~ blowing snow are more frequent than precipitation and mixed precipitation.

Figure 11 is similar to Figure 10 but for the entire Davos data set. In comparison with Figure 10, the occurrence of precipitation is much larger (and blowing snow much smaller), which is to be expected given the difference in geographic context (Alps vs Antarctica) and experimental set-up (wind-protected vs no wind shield). It should be noted that mixed cases are relatively frequent and that blowing snow still happens in Davos although the MASC was located in a wind shielding fence (DFIR).

~~The proposed method makes also possible the analysis of~~ Beyond global statistics on various data sets as presented above, the proposed approach can also be used to investigate the type of ~~particles~~ images at high temporal ~~resolution~~resolutions. Figure 12 shows an example of the output of the algorithm and corresponding images for a few time steps during a mixed event. It illustrates the capability of the proposed approach to distinguish blowing snow, precipitation and mixture in individual MASC images separated by a few ~~tenths to hundredths of seconds~~ seconds (and hence the contribution of the features other than image frequency). Over a longer time period, Figure 13 displays the evolution of the normalized angle for a mixed event

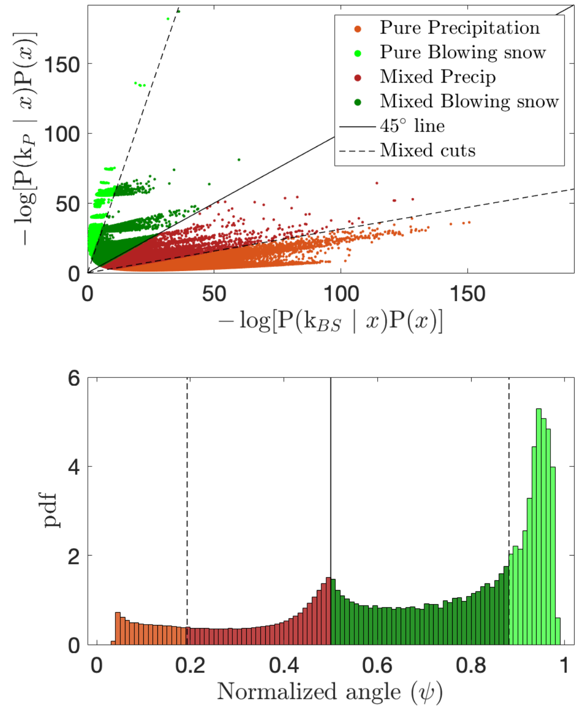

Figure 10. Top: scatter plot of the quadratic discriminant values of both components for the entire Antarctica 17 campaign. **Bottom**: distribution of the normalized angle and corresponding classification.

during the Antarctica 17 campaign. From roughly 09:00 to 12:00, the ~~type is dominantly~~ types precipitation and mixed are dominant, while between 12:00 and 14:00 the three types (precipitation, mixed, blowing snow) occur simultaneously. This is to be expected at DDU where katabatic winds blow very frequently, even during precipitation (e.g. Vignon et al., 2019). From 14:00 to 22:00, blowing snow becomes dominant (because of stronger winds). ~~Finally, after~~ After 22:00, mixed cases dominate and some images corresponding to precipitation are ~~even~~ detected towards the end of the event. The possibility to identify MASC images corresponding to precipitation, blowing snow or a mixture at a temporal resolution high enough to capture the dynamics of the event is an interesting feature for regions where both are frequently associated.

Considering the full Antarctic and Alpine data sets, it is interesting to analyze the potential differences in their characteristics. Figure 14 presents the distributions of the four descriptors as in Figure 6, but estimated from the entire data sets and not only the training sets (for images classified as pure blowing snow or pure precipitation). It can be seen that while the differences are limited for precipitation (slightly more frequent and larger in Davos than in Dumont d'Urville), they are significant for blowing snow: the blowing snow particles appear less fragmented (larger size and fractal index), less scattered within the images (larger distance transform) and with lower image frequencies in Davos. It should be recalled that the MASC was located in a wind-

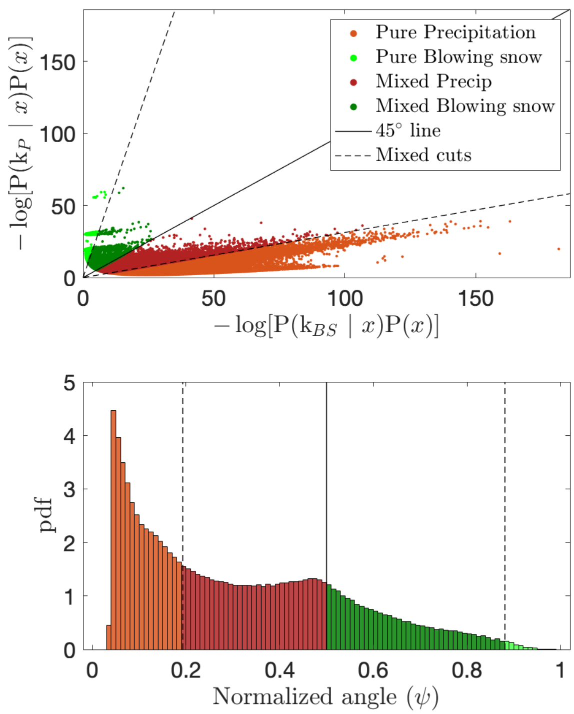

Figure 11. Same as Figure 10 for the entire Davos campaign.

protecting fence in Davos, so first the occurrence of blowing snow is much smaller (0.6 vs 36.5%), and second it is likely related to fresh snow blown away from the top of the nearby fence.

The MASC resolution ($33.5\,\mu\mathrm{m}$) and thresholding (minimum 3 pixels in area) during image processing lead to an image resolution not high enough to capture in full detail the geometry of blowing snow particles. It is nevertheless interesting to plot the distribution of the measured sizes (associated with the MASC sampling area) for blowing snow and precipitation cases and compare it to existing values in the literature. Figure 15 displays the distributions of the measured size (quantified here as D_{max}) for blowing snow and precipitation in Antarctica, as well as precipitation in the Swiss Alps. To help visualize the sometimes overlapping empirical distributions, the fitted Gamma distributions are also plotted. The units are given in $[\mathrm{mm}]$, with the approximation that one pixel is ~ 33.5 $[\mu\mathrm{m}]$.

As expected, the size distribution of blowing snow corresponds to smaller sizes than precipitation: the mode is around 0.2 $[\mathrm{mm}]$ for blowing snow and 0.3 to 0.4 $[\mathrm{mm}]$ for precipitation. More importantly, the right tail of the distribution is much larger for precipitation than for blowing snow. It should also be noted that the size is slightly larger in the Alpine data set (as illustrated by the slightly larger mode of the fitted Gamma distributions).

Timestamp	ID	Label	Normalized Angle	Mixing Index
25/03/2016 16:56:35	7383	1	0.7422	0.8178
25/03/2016 16:56:39	7384	0	0.1590	NaN
25/03/2016 16:56:39	7385	1	0.5659	0.5865
25/03/2016 16:56:40	7386	0	0.1437	NaN
25/03/2016 16:56:42	7387	0	0.1920	NaN
25/03/2016 16:56:42	7388	0	0.2260	0.0537

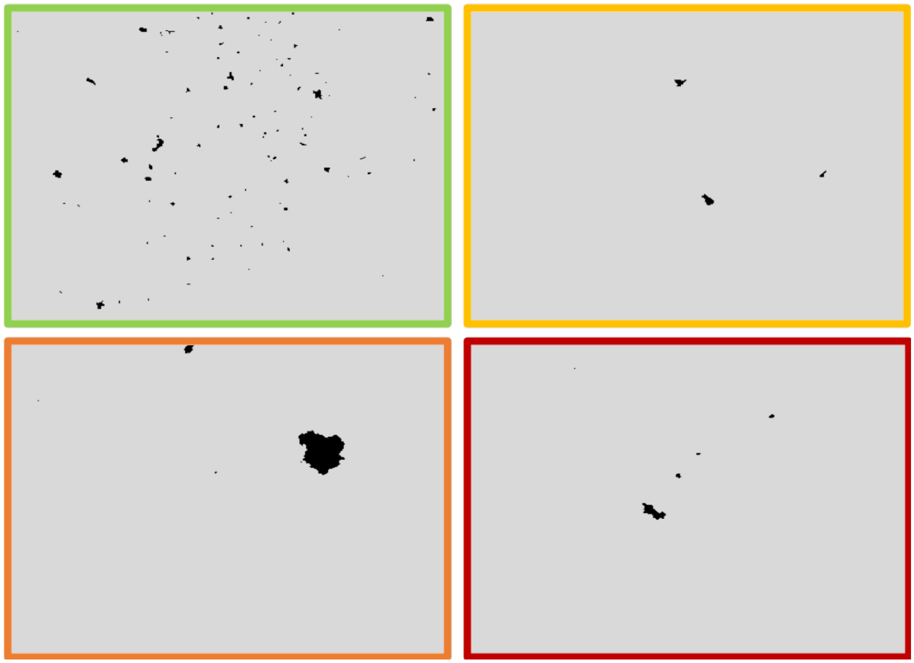

Figure 12. Consecutive MASC images from Davos and their respective classification label, normalized angle and mixing index. Label 1 is for blowing snow. A NaN mixing index means pure hydrometeor (or pure blowing snow). A mixing index close to 1 (top left image) means that it is near pure blowing snow, while a value close to 0 (bottom right image) indicate proximity to pure precipitation.

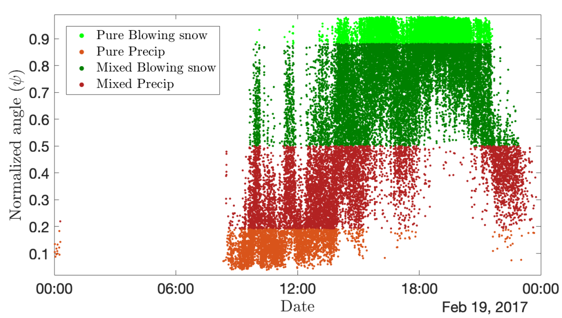

Figure 13. Time series of classified MASC images and corresponding ψ values (averaged over the three views) for a mixed event during the Antarctica 17 campaign.

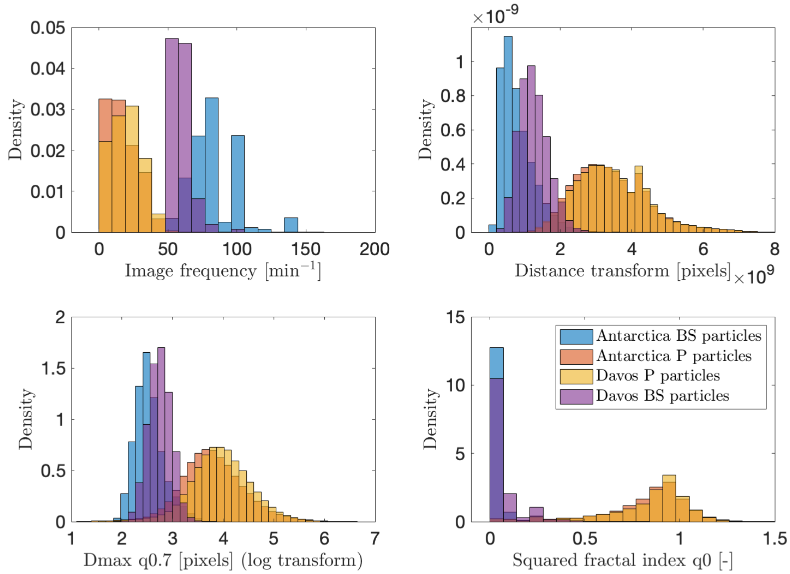

Figure 14. Histograms of selected descriptors for the training blowing snow and precipitation images from the entire Dumont d'Urville and Davos data sets.

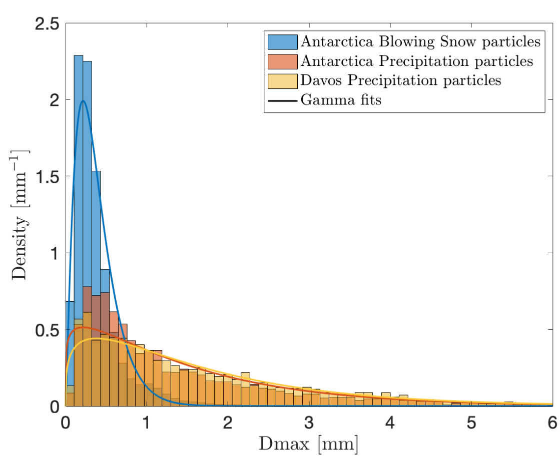

Figure 15. Histograms and fitted Gamma distributions of D_{max} for images classified as pure blowing snow and pure hydrometeors from Antarctica and pure precipitation from the Alps.

Nishimura and Nemoto (2005) provide size distributions of blowing snow and precipitation measured in Antarctica at Mizuho station using a SPC. The bimodality obtained when combining blowing snow and precipitation data in Figure 15 is in general agreement with the mixed case in their Figure 10. However, the mode for blowing snow appears at a lower size (below 50 [μm] in their Fig.7 at a height of 3.1 m). As mentioned before, this discrepancy is likely due to the limited effective resolution in MASC images after processing. In addition, as there are usually many particles in a single image during blowing snow, some may be out of focus and artificially appear larger than they are. So we expect the blowing snow features extracted from MASC data to be biased towards larger particles. It should also be noted that the sampling areas of the two instruments are different (see Section 2.1) and this could partly explain the differences in the obtained distributions.

Overall, it appears that the MASC images, processed as explained in Praz et al. (2017), are not adapted to a detailed study of the geometry of blowing snow particles, but are still relevant to distinguish blowing snow and precipitation, to characterize mixtures of both and to analyze the dynamics of blowing snow at high temporal resolutions.

6 Conclusions

A novel method to automatically detect images from the MASC instrument corresponding to blowing snow is introduced. ~~The classification is achieved by a two components Gaussian mixture model fitted on a subset of 8450 representative images from field campaigns in Antarctica and Davos, Switzerland.~~ To classify the images, the method computes four selected descriptors via image processing. The descriptors were selected to be relevant for discriminating between blowing snow particles and hydrometeors as well as to be robust to image processing artifacts. The classification is achieved by a two-component Gaussian mixture model fitted on a subset of 8450 representative images from field campaigns in Antarctica and Davos, Switzerland. The fitted GMM is shown to reliably distinguish images corresponding to pure blowing snow and pure precipitation cases. The GMM posterior probabilities are also mapped into a new index that allows a better identification of mixed images and a flag signals whether an image is classified as pure hydrometeor, pure blowing snow or mixed. For mixed images, an index between 0 and 1 ~~indicates~~ is proposed to indicate if the image is closer to blowing snow or precipitation. Its evaluation remains qualitative as there are no quantitative observations that can be used as reference for mixed cases. The outputs are provided for each image independently or for each triplet of images (i.e. information combined over the three cameras of the MASC).

Results from a measurement campaign conducted at the Dumont d'Urville station on the coast of East Antarctica from January to July 2017 suggest that about 75% of the images are affected by blowing snow and that about 36% may be composed of blowing snow particles only (Table 3). The results also suggest that about 56% of the images could be made of a mix of blowing snow and precipitation particles, which support findings that in Antarctica, blowing snow is frequently combined with precipitation (e.g. Gossart et al., 2017). Moreover, time series of the classified images highlight that blowing snow strongly relies upon fresh snow availability and often starts shortly after the beginning of precipitation (Fig.13), which is also consistent with conclusions from Gossart et al. (2017). Results from images taken inside a Double Fence Intercomparison Reference in Davos at 2540 m a.s.l between December 2015 and March 2016, indicate that despite the sheltering structure, about 60% of the images could be affected to some extent by blowing snow particles from adjacent fence ledges. In terms of percentage of images, these numbers tend to be quite large, as the image frequency is usually much higher when strong blowing snow occurs, but the occurrence is more balanced in terms of time.

As the method was developed and tested on fundamentally different campaigns, it may have a general applicability to any other MASC images. However, it should be noted that some descriptors depends on the particular settings (e.g. image size, pixel resolution) used during the aforementioned campaigns and a new GMM should be fitted if different settings apply. Further work should be conducted to evaluate if the method can give satisfactory results on images that do not include a timestamp, as the image frequency descriptor could not be utilized. In this case, it could be replaced by one or a couple of other descriptors listed in Table A.1 of Appendix A to strengthen the model. The method could also be adjusted to train a model with a supervised learning algorithm that provides posterior probabilities such as Bayesian classifiers or logistic regression. However, this would imply some effort to increase the training set. An inter-comparison between different machine learning algorithms and the creation of different validation sets could help gain confidence in the results.

The main limitations of the present method are the assumption of normally distributed features through the use of the GMM, the too-coarse resolution of the MASC to properly capture the small end of the distribution of blowing snow particle size, and the dependency of the method on the defined training set. The latter illustrates the problem of generalization. Some extremely high intensity snowfall events, higher than the ones observed during the Davos and Antarctica campaigns, could be erroneously classified as blowing snow with the current model due to the nature of the descriptors. In this case, higher intensity pure snowfall events should be included in the training set. Another example is the size of the blowing snow particles. During the campaigns in Antarctica, the MASC was set up on a rooftop at $3\,\mathrm{m}$ a.g.l. Several studies have demonstrated that the size of blowing snow particles tends to decrease with height (Nishimura and Nemoto, 2005; Nishimura et al., 2014). Consequently, blowing snow particles on images from a MASC that would have been set up at much higher or lower heights may have a bias relative to the fitted Gaussian distribution of the Blowing Snow cluster for *Dmax*. It is thus recommended to follow the procedure described in this article and fit a new model, if the one provided does not perform well in other contexts.

Appendix A: Feature extraction

Table A1. Full list of all computed descriptors. Descriptors related to each particle are transformed into a single descriptor for the image (right column). Selected ones are shown with an asterisk

Image frequency*	-
Number of particles detected in the image	-
Distance to connect all particles	-
Number of particles smaller than a given threshold	-
Ratio of the area represented by all particles to the area of the smallest polygon encircling them	-
Cumulative distance transform*	-
Maximum diameter*	quantiles 0-1, Moments 1-5
Particle area	quantiles 0-1, Moments 1-5
Particle convex area	quantiles 0-1, Moments 1-5
Particle perimeter	quantiles 0-1, Moments 1-5
Fractal Index (FRAC), Fractal Index squared*	quantiles 0-1, Moments 1-5
Gravelius compactness coefficient (ratio of the perimeter to the one of a circle with equivalent area)	quantiles 0-1, Moments 1-5

Appendix B: Image processing issues

The median filter may perform not satisfactorily, for instance when the background luminosity is changing rapidly (see Fig. B1).

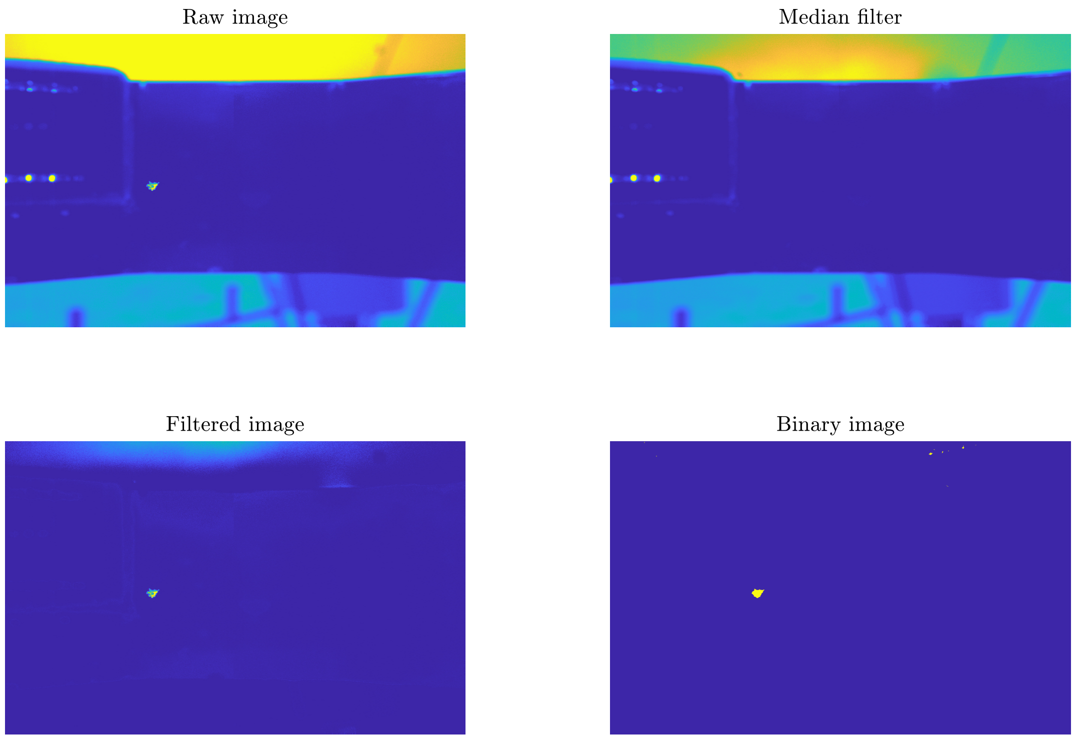

Figure B1. Raw image, median filter, filtered image and final binary image for an example where the median filter does not perform well due to changes in sky luminosity. Some artifacts appear on the top right of the binary image

Similarly, large precipitation particles may split or appear as such in the MASC images (see Fig. B2), leading to potential biases in the number of detected particles.

Code availability. TEXT

Data availability. TEXT

Code and data availability. The MASC images and the matlab codes used in the present work are available upon request to the authors.

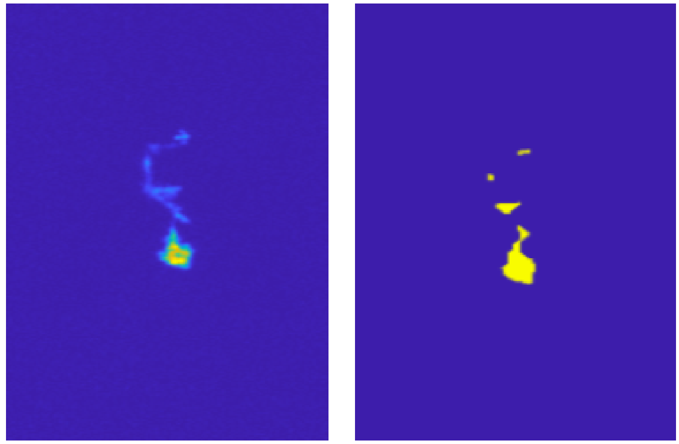

Figure B2. A precipitation particle split into fragments that could be confused with blowing snow particles. The Cumulative distance transform descriptor is much less affected by such image processing issues than the number of particles.

Sample availability. TEXT

Author contributions. TEXT

Competing interests. The authors have no competing interests

Disclaimer. TEXT

Acknowledgements. The authors are thankful to Yves-Alain Roulet and Jacques Grandjean from MeteoSwiss, as well as to Claudio Dùran from IGE Grenoble and to the technical staff at the Dumont d'Urville station for their help to collect the set of MASC images used in this study. CP was supported by the Swiss National Science Foundation (grant 200020_175700).

References

Bellot, H., Trouvilliez, A., Naaim-Bouvet, F., Genthon, C., and Gallée, H.: Present weather-sensor tests for measuring drifting snow, Adv. Geophys., 52, 176–184, 2011.

Bintanja, R.: Snowdrift sublimation in a katabatic wind region of the Antarctic ice sheet, J. Appl. Meteorol., 40, 1952–1966, https://doi.org/10.1175/1520-0450(2001)040<1952:SSIAKW>2.0.CO;2, 2001.

Box, J. E., Bromwich, D. H., Veenhuis, B. A., Bai, L.-S., Stroeve, J. C., Rogers, J. C., Steffen, K., Haran, T., and Wang, S.-H.: Greenland ice sheet surface mass balance variability (1988–2004) from calibrated polar MM5 output, J. Climate, 19, 2783–2800, 2006.

Budd, W., Dingle, W., and Radok, U.: The Byrd snow drift project: outline and basic results, in: Studies in Antarctic Meteorology, edited by Rubin, M. J., vol. 9 of *Antarctic Research Series*, pp. 71–134, American Geophysical Union, 1966.

Budd, W. F.: The drifting of non-uniform snow particles, in: Studies in Antarctic Meteorology, edited by Rubin, M. J., vol. 9 of *Antarctic Research Series*, pp. 59–70, American Geophysical Union, 1966.

Byrt, T., Bishop, J., and Carlin, J. B.: Bias, prevalence and kappa, J. Clin. Epidemiol., 46, 423–429, 1993.

Comola, F., Kok, J. F., Gaume, J., Paterna, E., and Lehning, M.: Fragmentation of wind-blown snow crystals, Geophys. Res. Lett., 44, 4195–4203, 2017.

Crivelli, P., Paterna, E., Horender, S., and Lehning, M.: Quantifying particle numbers and mass flux in drifting snow, Bound.-Lay. Meterol., 161, 519–542, 2016.

Das, I., Bell, R. E., Scambos, T. A., Wolovick, M., Creyts, T. T., Studinger, M., Frearson, N., Nicolas, J. P., Lenaerts, J. T. M., and van den Broeke, M. R.: Influence of persistent wind scour on the surface mass balance of Antarctica, Nat. Geosci., 6, 367–371, https://doi.org/10.1038/NGEO1766, 2013.

De Maesschalck, R., Jouan-Rimbaud, D., and Massart, D. L.: The Mahalanobis distance, Chemometr. Intell. Lab., 50, 1–18, 2000.

Déry, S. J. and Yau, M.: Large-scale mass balance effects of blowing snow and surface sublimation, J. Geophys. Res., 107, ACL–8, 2002.

Ehbrecht, M., Schall, P., Ammer, C., and Seidel, D.: Quantifying stand structural complexity and its relationship with forest management, tree species diversity and microclimate, Agr. and Forest Meteor., 242, 1–9, 2017.

Gallée, H., Guyomarc'h, G., and Brun, E.: Impact of snow drift on the Antarctic ice sheet surface mass balance: possible sensitivity to snow-surface properties, Bound.-Lay. Meterol., 99, 1–19, 2001.

Garrett, T. J., Fallgatter, C., Shkurko, K., and Howlett, D.: Fall speed measurement and high-resolution multi-angle photography of hydrometeors in free fall, Atmos. Meas. Tech., 5, 2625–2633, https://doi.org/10.5194/amt-5-2625-2012, 2012.

Garrett, T. J., Yuter, S. E., Fallgatter, C., Shkurko, K., Rhodes, S. R., and Endries, J. L.: Orientations and aspect ratios of falling snow, Geophys. Res. Lett., 42, 4617–4622, 2015.

Genthon, C., Berne, A., Grazioli, J., Alarcon, C. D., Praz, C., and Boudevillain, B.: Precipitation at Dumont d'Urville, Adélie Land, East Antarctica: the APRES3 field campaigns dataset, Earth Syst. Sci. Data, 10, 1605–1612, https://doi.org/10.5194/essd-10-1605-2018, 2018.

Goodison, B. E., Louie, P. Y., and Yang, D.: WMO solid precipitation measurement intercomparison, World Meteorological Organization Geneva, Switzerland, 1998.

Gordon, M. and Taylor, P. A.: Measurements of blowing snow, Part I: Particle shape, size distribution, velocity, and number flux at Churchill, Manitoba, Canada, Cold Reg. Sci. Technol., 55, 63–74, 2009.

Gossart, A., Souverijns, N., Gorodetskaya, I. V., Lhermitte, S., Lenaerts, J. T., Schween, J. H., Mangold, A., Laffineur, Q., and van Lipzig, N. P.: Blowing snow detection from ground-based ceilometers: application to East Antarctica, The Cryosphere, 11, 2755, https://doi.org/10.5194/tc-11-2755-2017, 2017.

Grazioli, J., Genthon, C., Boudevillain, B., Duran-Alarcon, C., Del Guasta, M., Madeleine, J.-B., and Berne, A.: Measurements of precipitation in Dumont d'Urville, Adélie Land, East Antarctica, The Cryosphere, 11, 1797–1811, https://doi.org/10.5194/tc-11-1797-2017, https://www.the-cryosphere.net/11/1797/2017/, 2017.

Guyomarc'h, G., Bellot, H., Vionnet, V., Naaim-Bouvet, F., Déliot, Y., Fontaine, F., Puglièse, P., Nishimura, K., Durand, Y., and Naaim, M.: A meteorological and blowing snow data set (2000–2016) from a high-elevation alpine site (Col du Lac Blanc, France, 2720 m asl), Earth Syst. Sci. Data, 11, 57–69, 2019.

Kennedy, P., Thurai, M., Praz, C., Bringi, V., Berne, A., and Notaroš, B. M.: Variations in Snow Crystal Riming and Z DR: A Case Analysis, J. Appl. Meteor. Clim., 57, 695–707, 2018.

Kimura, F., Takashina, K., Tsuruoka, S., and Miyake, Y.: Modified quadratic discriminant functions and the application to Chinese character recognition, IEEE T. Pattern Anal., pp. 149–153, 1987.

Kinar, N. and Pomeroy, J.: Measurement of the physical properties of the snowpack, Rev. Geophys., 53, 481–544, 2015.

Kind, R. J.: Mechanics of aeolian transport of snow and sand, JWEIA, 36, 855–866, 1990.

Lehning, M. and Fierz, C.: Assessment of snow transport in avalanche terrain, Cold Reg. Sci. Technol., 51, 240–252, 2008.

Lenaerts, J. T. M. and van den Broeke, M. R.: Modeling drifting snow in Antarctica with a regional climate model: 2. Results, J. Geophys. Res., 117, https://doi.org/10.1029/2010JD015419, 2012.

Leonard, K. C., Tremblay, L.-B., Thom, J. E., and MacAyeal, D. R.: Drifting snow threshold measurements near McMurdo station, Antarctica: A sensor comparison study, Cold Reg. Sci. Technol., 70, 71–80, 2012.

Lesins, G., Bourdages, L., Duck, T., Drummond, J., Eloranta, E., and Walden, V.: Large surface radiative forcing from topographic blowing snow residuals measured in the High Arctic at Eureka, Atmos. Chem. Phys., 2009.

McGarigal, K. and Marks, B. J.: Spatial pattern analysis program for quantifying landscape structure, Tech. Rep. Gen. Tech. Rep. PNW-GTR-351, US Department of Agriculture, Forest Service, Pacific Northwest Research Station, 1995.

McLachlan, G. J. and Basford, K. E.: Mixture models: Inference and applications to clustering, vol. 84, Wiley Online Library, 1988.

Moerland, P.: Mixture models for unsupervised and supervised learning, 2000.

Mott, R. and Lehning, M.: Meteorological Modeling of Very High-Resolution Wind Fields and Snow Deposition for Mountains, JHM, 11, 934–949, https://doi.org/10.1175/2010JHM1216.1, 2010.

Murphy, K. P.: Machine Learning: A Probabilistic Perspective, MIT Press, 2012.

Naaim-Bouvet, F., Bellot, H., Nishimura, K., Genthon, C., Palerme, C., Guyomarc'h, G., and Vionnet, V.: Detection of snowfall occurrence during blowing snow events using photoelectric sensors, Cold Reg. Sci. Technol., 106, 11–21, 2014.

Nishimura, K. and Nemoto, M.: Blowing snow at Mizuho station, Antarctica, Philos. T. Roy. Soc. A, 363, 1647–1662, 2005.

Nishimura, K., Yokoyama, C., Ito, Y., Nemoto, M., Naaim-Bouvet, F., Bellot, H., and Fujita, K.: Snow particle speeds in drifting snow, J. Geophys. Res., 119, 9901–9913, 2014.

Palm, S. P., Yang, Y., Spinhirne, J. D., and Marshak, A.: Satellite remote sensing of blowing snow properties over Antarctica, J. Geophys. Res., 116, –, https://doi.org/10.1029/2011JD015828, 2011.

Pomeroy, J. and Li, L.: Prairie and arctic areal snow cover mass balance using a blowing snow model, J. Geophys. Res., 105, 26 619–26 634, 2000.

Praz, C., Roulet, Y.-A., and Berne, A.: Solid hydrometeor classification and riming degree estimation from pictures collected with a Multi-Angle Snowflake Camera, Atmos. Meas. Tech., 10, 1335–1357, https://doi.org/10.5194/amt-10-1335-2017, 2017.

Rasmussen, R., Baker, B., Kochendorfer, J., Meyers, T., Landolt, S., Fischer, A. P., Black, J., Thériault, J. M., Kucera, P., Gochis, D., Smith, C., Nitu, R., Hall, M., Ikeda, K., and Gutmann, E.: How well are we measuring snow: The NOAA/FAA/NCAR winter precipitation test bed, Bull. Amer. Meteor. Soc., 93, 811–829, https://doi.org/10.1175/BAMS-D-11-00052.1, 2012.

Scaff, L., Yang, D., Li, Y., and Mekis, E.: Inconsistency in precipitation measurements across the Alaska–Yukon border, The Cryosphere, 9, 2417–2428, 2015.

Scarchilli, C., Frezzotti, M., Grigioni, P., De Silvestri, L., Agnoletto, L., and Dolci, S.: Extraordinary blowing snow transport events in East Antarctica, Clim. Dynam., 34, 1195–1206, https://doi.org/10.1007/s00382-009-0601-0, 2010.

Schmidt, R.: Threshold wind-speeds and elastic impact in snow transport, J. Glaciol., 26, 453–467, 1980.

Schweizer, J., Bruce Jamieson, J., and Schneebeli, M.: Snow avalanche formation, Rev. Geophys., 41, 2003.

Shepherd, A., Ivins, E. R., Geruo, A., Barletta, V. R., Bentley, M. J., Bettadpur, S., Briggs, K. H., Bromwich, D. H., Forsberg, R., Galin, N., et al.: A reconciled estimate of ice-sheet mass balance, Science, 338, 1183–1189, 2012.

Vignon, É., Traullé, O., and Berne, A.: On the fine vertical structure of the low troposphere over the coastal margins of East Antarctica, Atmos. Chem. Phys., 19, 4659–4683, 2019.

Winstral, A., Elder, K., and Davis, R. E.: Spatial snow modeling of wind-redistributed snow using terrain-based parameters, J. Hydrometeorol., 3, 524–538, 2002.

Yang, Y., Palm, S. P., Marshak, A., Wu, D. L., Yu, H., and Fu, Q.: First satellite- detected perturbations of outgoing longwave radiation associated with blowing snow events over Antarctica, Geophys. Res. Lett., 41, 730–735, https://doi.org/10.1002/2013GL058932, 2014.